Particulate Airborne Impurities

Express Analysis and Health Effects

Kai Wilkinson
Faculty of Natural Resources and Agricultural Sciences
Department of Chemistry
Uppsala

Doctoral Thesis
Swedish University of Agricultural Sciences
Uppsala 2013

Acta Universitatis agriculturae Sueciae
2013:27

Cover: Digitally generated image of a LEGO-brick factory where the design of magnetite nanoparticles takes place. Borders are actual magnetite particles with some showing a fringe-pattern. Software used: LDD 4.3, MLCAD 3.40, LDView 4.1, and POVRay 3.6.
(Image: Wilkinson, Kai)

ISSN 1652-6880
ISBN 978-91-576-7792-1 (electronic) 978-91-576-7793-8

Print: SLU Repro, Uppsala 2013

Particulate Airborne Impurities: Express Analysis and Health Effects

Abstract

The cumulative effects of air pollutants are of principal concern in research on environmental protection in Sweden. Post-industrial society has imposed many limits on emitted air pollutants, yet the number of reports on the negative effects from them is increasing, largely due to human activity in the form of industrial emissions and increased traffic flows. Rising concerns over the health effects from airborne particulate matter (PM) stem from *in vitro*, *in vivo*, and cohort studies revealing effects of mostly negative nature.

Full insight into the health effects from PM can only be achieved through practical investigation of the mode of toxicity from distinct types of particles and requires techniques for their identification, monitoring, and the production of model fractions for health studies.

To this effect, comprehensive collection and chemical analysis of particulates at the origin of emission was performed in order to provide clearer insight into the nature of the particulates at exposure and add detail to aid risk assessment. Methods of capturing particles and analyzing their chemical nature were devised using scanning electron microscopy coupled with energy dispersive spectroscopy (SEM-EDS).

Furthermore, taking the approach of *in vitro* cytotoxicity testing, nanoparticles of types typical to automotive emissions, were synthesized and extensively characterized using SEM-EDS, X-ray diffraction (XRD), transmission electron microscopy (TEM), dynamic light scattering (DLS), and nanoparticle tracking analysis (NTA). The produced model magnetite and palladium nanoparticles were found to induce toxicity in human pulmonary epithelial cells (A549 and PBEC) as well as impact severely on immunological and renal cells (221 B- and 293T-cells) in a dose-dependent manner.

Keywords: air pollution, particulate matter, PM, nanoparticle, toxicity, monitoring, SEM-EDS, TEM

Author's address: Kai Wilkinson, SLU, Department of Chemistry,
P.O. Box 7015, 750 07 Uppsala, Sweden
E-mail: kai.wilkinson@slu.se

Dedication

For my loving family

I don't like to commit myself about heaven and hell, you see, I have friends in both places.
- Mark Twain

The Iron never lies to you. You can walk outside and listen to all kinds of talk, get told you're a god or a total bastard. The Iron will always kick you the real deal. The Iron is the great reference point, the all-knowing perspective giver. Always there like a beacon in the pitch black. I have found the Iron to be my greatest friend. It never freaks out on me, never runs. Friends may come and go. But two hundred pounds is always two hundred pounds.
- Henry Rollins

Contents

List of Publications

This thesis is based on the work contained in the following papers, referred to by Roman numerals in the text:

I Wilkinson, K; Lundkvist, J.; Seisenbaeva, G; Kessler, V. (2011). New Tabletop SEM-EDS-Based Approach for Cost-Efficient Monitoring of Airborne Particulate Matter. *Environ Pollut* 159, 311-318.

II Wilkinson, K.; Lundkvist, J.; Netrval, J.; Eriksson, M.; Seisenbaeva, G.; Kessler, V. Space and Time Resolved Monitoring of Airborne Particulate Matter in Proximity of a Traffic Roundabout in Sweden (submitted manuscript).

III Wilkinson, K. E.; Palmberg, L.; Witasp, E.; Kupczyk, M.; Feliu, N.; Gerde, P.; Seisenbaeva, G. A.; Fadeel, B.; Dahlén, S.-E.; Kessler, V. G. (2011). Solution-Engineered Palladium Nanoparticles: Model for Health Effect Studies of Automotive Particulate Pollution. *ACS Nano* 5(7), 5312-5324.

IV Wilkinson, K.; Ekstrand-Hammarström, B.; Ahlinder, L.; Guldevall, K.; Pazik, R.; Kepinski, L.; Kvashnina, K. O.; Butorin, S. M.; Brismar, H.; Önfelt, B.; Österlund, L.; Seisenbaeva, G. A.; Kessler, V. G. (2012). Visualization of Custom-Tailored Iron Oxide Nanoparticles Chemistry, Uptake, and Toxicity. *Nanoscale* 4(23), 7383-7393.

The contribution of Kai Wilkinson to the papers included in this thesis was as follows:

I Collection of particles together with Vadim Kessler and Anders Gambe. SEM-EDS Analysis of particles together with Johanna Lundkvist. Main- and corresponding author of the paper.

II Collection of particles together with Johanna Lundkvist. Analysis of particles together with Julia Netrval and Mats Eriksson. Data analysis and writing the paper. Main- and corresponding author of the paper.

III Synthesis of Pd- and Pd/Al-NPs and the characterization of these using X-ray crystallography, transmission electron microscopy, thermal gravimetric analysis, dynamic light scattering, and nanoparticle tracking analysis with certain help from others. Interpretation of data and writing main body of text for the paper.

IV Synthesis of iron oxide NPs and the characterization of these using X-ray crystallography, transmission electron microscopy, thermal gravimetric analysis, dynamic light scattering, and nanoparticle tracking analysis with certain help from others. Interpretation of data and writing main body of text for the paper.

Abbreviations

221	Human Epstein-Barr-virus transformed 721.221 B-cell
293T	Adherent human embryonic kidney HEK293T-cell
A549	Transformed adenocarcinomic human alveolar basal epithelial cell
acac	Acetylacetonate
ALD	Atomic layer deposition
ANOVA	Analysis of variance
at%	Atomic-percent
ATP	Adenosine-tri-phosphate
BAL	Bronchoalveolar lavage
BSE	Backscattered electron
CCD	Charge-coupled device
CFC	Chlorofluorocarbons
DEVD-AMC	(Asp-Glu-Val-Asp)-7-amino-4-methylcoumarin
df / Df	Degrees of freedom. Indexes: error (degrees of freedom for SS_{error} calculation)
DLS	Dynamic light scattering
DMSO	Di-methyl sulfoxide
DNA	Does not apply
EDS	Energy dispersive spectroscopy
EEA	European environment agency
ELISA	Enzyme-linked immunosorbent assay
EM	Electron Microscopy
EPA	U.S. environmental protection agency
EU	European union
FAAS	Flame absorption atomic spectroscopy
FCS	Fetal calf serum
FeO_x	Iron oxides

FIB	Focused ion beam
FT	Fourier transform
FWHM	Full width at half maximum
GC	Gas chromatography
ICP	Inductively coupled plasma
IL-8	Interleukin-8
IR	Infrared
LSD	Least significant difference
Mean-sq	Mean sum-of-squares
MRI	Magnetic resonance imaging
MS	Mass spectrometry
NIPALS	Non-linear iterative projections by alternating least-squares
NO_x	Nitrogen oxides
NP	Nanoparticle
NTA	Nanoparticle tracking analysis
RPMI	Roswell park memorial institute medium
PBEC	Primary human bronchial epithelial cell
PC	Principal component
PCA	Principal component analysis
PM	(Airborne) particulate matter. Indexes: *1*, *2.5*, and *10* (particulate matter with an aerodynamic diameter of less than 1, 2.5, and 10 μm respectively)
PMG	Platinum metal group
Pr	Probability
ROS	Reactive oxygen species
SAD	Selected area diffraction
SDD	Silicon drift detector
SE	Secondary electron
SEM	Scanning electron microscopy
SO_x	Sulfur oxides
SS / Sum-sq	Sum of squares. Indexes: *i* (SS of *i* groups of data), *error* (SS of the error of *i*), *among* (SS among groups)
STEM	Scanning-transmission electron microscopy
STS	Staurosporine
TEM	Transmission electron microscopy
TiO_x	Titanium oxides
(U)SPION	(Ultrasmall) superparamagnetic iron oxide nanoparticle
VOC	Volatile organic compounds
VTI	The Swedish national road and transport research institute
WHO	World health organization

wt%	Weight-percent
XPD	X-ray powder diffraction

1 A brief introduction

The earliest evidence of human exposure to harmful inhalable particulate matter come by way of Ötzi the iceman. Ötzi was a 45 year old late Neolithic/ early Calcolithic man who met his demise by acts of violence some 5,300 years ago [Pernter 2007]. His remains were found by pure chance in 1991 by a pair of hikers in the Italian Alps. Subsequent analyses of his well preserved remains have given an unprecedented view of the lifestyle of him and his contemporaries. Analysis of his lungs proved that they were covered in, among other things, aluminosilicate mineral and fine soot particles originating most probably from breathing in smoke from camp fires and threshing food preparation [Pabst 1998]. Additionally his hair contained elevated amounts of copper, most probably from the exposure of fumes from metallurgic handling of this metal, indicating that technogenic particulate pollution already played a considerable role in health at that time.

Irrespective of the time that has passed people today are still exposed to the same environmental conditions, particularly in many third world countries where the burning of biofuels for heating and food preparation is commonplace [Ludwig 2003].

Knowledge of the harmful effects of inhalable particulates was commonly shared for a long time as it was tied to traditional occupations such as metal smiths. London in 1273 was a burgeoning city and the practice of burning wood was being replaced by that of burning coal. It is thought that the sulfur content was high in the sea-coal that was predominantly being used and produced harmful emissions of gases and smog. King Edward I declared:

> ´Be it known to all within the sound of my voice, whosoever shall be found guilty of the burning of coal shall suffer the loss of his head.´

Soon laws were passed to limit the coal use and these were by and large ignored.

The burning of coal still played a big part in harmful emissions. By the end of the 19th century when industrialization was booming new laws were being filed to limit industrial emissions. An event called The Great London Smog in 1952, caused by a series of weather conditions leading to accumulated emissions over the city of London directly resulted in around 4,000 dead and another 100,000 suffering from respiratory illnesses. A milestone in legislation occurred shortly after in 1956 and -68 when The Clean Air Act was passed, detailing among other things that chimneys and smoke stacks should be used by the industry to disperse emissions over a larger area, effectively diluting the smog in the air.

Air quality was improved but still far from ideal. The emergence in numbers and use of automobiles aggravated the air quality once more. The amount of vehicles operating on fossil fuels increased exponentially and smog started to reappear across the world in the late 1970's. The sulfur content of fuels was largely in control, but new emissions appeared: lead, nitrous oxides, ozone, and effects such as photochemical smog (chemical reactions on gas emissions caused by sunlight). A number of measures were taken to limit emissions: removal of lead from fossil fuels, introduction of catalytic converters, and furthermore limiting the emissions from industry and energy production.

By the 21st century air quality was much improved although the discussion on the greenhouse effect was gaining momentum. Regardless of source most scientists agree that elevated levels of greenhouse gases (*e.g.* carbon dioxide, methane) are causing entrapment of thermal radiation in the earths' lower atmosphere and thus elevating the global mean temperature. The rising temperature has implications on the ecosystem as a sudden increase will change the configuration of the biosphere leading to *e.g.* food shortages from diminished crop yields. Additionally airborne particulate matter has been reported to amount to approximately 25% of the greenhouse effect due to global dimming, or as much as 50% locally in certain highly polluted places [Bond 2007].

It is clear that our way of life is strongly associated with emissions of harmful pollutants, particularly that of air pollution. The attention to air pollutants has strongly increased during recent years. Two factors play a major role in this development: recognition of the serious influence of particulate impurities on human health and the understanding of the effect of airborne particles on local and global climate change. Despite limitations and legislation the amounts of pollutants is increasing and with those the associated negative health effects. There is much more to be done so that we can attain a sustainable society and maintain a small ecological imprint to lead

a healthier way of life. Therefore the aim of the current work was to develop techniques for fast identification of particles on a chemical level for quantification in on-site monitoring and use representative fractions of particles for *in vitro* testing to ascertain their mode of toxicity improving our understanding of how we as humans are affected by them.

2 Scientific aims

In the frame of the present thesis the following aims were pursued: To develop a new reliable approach to quick and cost-efficient monitoring of particulate matter by: I) determining the chemical constituents of individual particles and their relation to health risks from a risk-assessment point of view, II) make monitoring cost-effective using newly developed miniaturized scanning electron microscopy, and III) develop methods of source apportionment of particles.

In addition methods of synthesizing nanoparticles as a model for ultrafine particles were devised to mimic emissions from vehicular traffic. These were characterized extensively using transmission electron microscopy, X-ray powder crystallography, nanoparticle tracking analysis, and dynamic light scattering.

The main aim was to identify the potentially most chemically active components in airborne particulate matter and use model *in vitro* systems to evaluate their health effects.

3 Background

The research presented in the present thesis was built on the vast volume of literature data available on the nature of particulate air pollution, monitoring, legislation, and the health effects of those.

3.1 Particulate air pollution

Air pollution comes in many forms: gases, liquids, and/or particulates suspended in air. An aerosol is defined as particulates and liquids suspended together. Airborne particulate matter (PM) describes the solid matter suspended in air, although gases and liquids can be adsorbed on PM, and no distinction is made for these. Most PM is produced directly at the emission source but some can form *post factum* by indirect chemical reactions [Foltescu 1996]. Table 1 lists an overview of the most abundant air pollutants. In this thesis the focus is set on inorganic PM.

Table 1. *List of the most common air pollutants [Fox 1997].*

Pollutant	Description	Source
SO_x	Sulfur oxides	Natural (volcano ash), coal combustion, industrial
NO_x	Nitrogen oxides	High-temperature combustion
CO	Carbon monoxide	Incomplete combustion of bio- and fossil fuels
CO_2	Carbon dioxide	Combustion and respiration (from biosphere)
VOC	Volatile organic compounds	By-product of combustion
PM	Particulate matter	Natural (fires, volcano, dust), combustion
CFC	Chlorofluorocarbons	Not in use anymore, persistent
NH_3	Ammonia	Agricultural use
O_3	Ground-level ozone	Indirectly formed from VOCs and NO_x

3.1.1 PM behaviour and prevalence

Naturally occurring PM can be attributed to originating from natural sources, *i.e.* is ambiently suspended in air as a background concentration stemming from sea-spray, surface erosion, and vegetation [Perrino 2008]. Other natural sources such as dust storms, volcano eruptions, and forest fires can greatly exacerbate the amount of PM in the air [Ilyinskaya 2012, Price 2012, Lazaridis 2008]. There is a strong correlation with the increasing population on earth, industrialization and PM pollution [Fenger 1999]. PM is classified by its size mode: PM_{10} denotes particles that are 10 μm or less in diameter and are sometimes called coarse particles; $PM_{2.5}$ denotes particles that are 2.5 μm or less in diameter and are sometimes called fine particles; PM_1 are particles that are 1 μm or less in diameter and are sometimes called ultrafine particles. In ambient air they typically conform to a size distribution as seen in Figure 1. As PM is dispersed in air it can be transported by wind and diffusion, so locally emitted pollution is in effect a global problem [Isakson 1997].

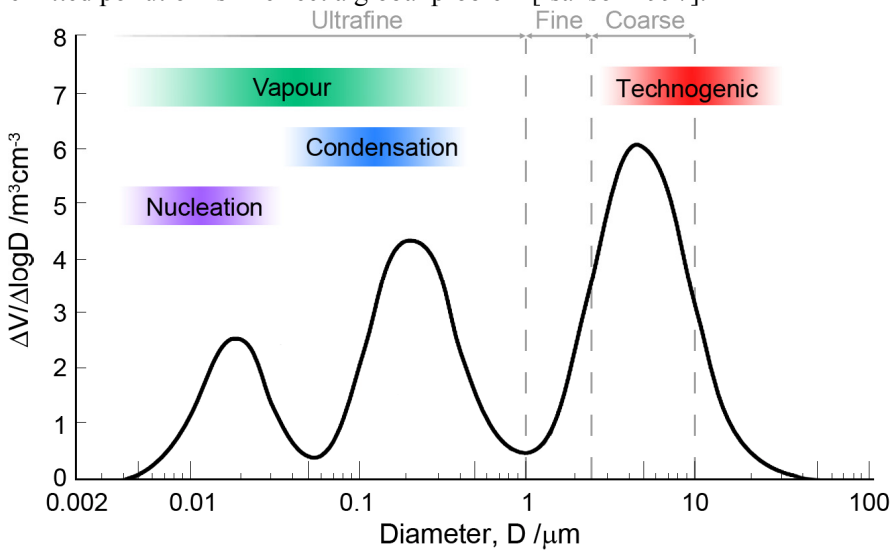

Figure 1. Volume-size distribution of measured aerosol with sources of accumulation. Grey lines show the Coarse (PM_{10}), Fine ($PM_{2.5}$), and Ultrafine (PM_1) size modes. From [U.S. EPA 1996].

Roadside emissions of PM can originate in part from mechanical and tire wear or combustion particulates. The Swedish National Road and Transport Research Institute (VTI) have reported on the wear from road materials, giving rise to emissions of PM_{10} with significant amounts of silicates and associated minerals dependent on the materials used in the construction of roads [Gustafsson 2011]. Notwithstanding the PM_{10} emissions, the fine and ultrafine

size modes are present and in elevated levels in conjunction with the use of studded tires during winter road conditions.

3.1.2 Nanoparticles

Nanomaterials are defined per the European Commision (2011) as being matter with at least one dimension between 1 and 100 nm [Genzleben 2011]. For practical reasons nanoparticles (NP) are seen as nanomaterials but are usually constrained to having all dimensions less than 100 nm. NPs are mostly devoid in nature, only originating from high temperature combustion, high energy kinetic effects, or originating from engineered sources [Giordano 2010, Silva 2011]. Nanomaterials are a novel material[1] in terms of industrial production and commercial use as their inherently small size gives them properties that are not usually present in the bulk material, such as a depression in the melting point of NPs as compared to the bulk material giving them a wide range of applications [Sun 2007]. Novel uses of NPs include sports equipment (carbon nanotubes packed in a polymer composite for tennis rackets, Ag-NPs as disinfectant in clothes), catalysts (Pd/Pt-NPs in automobile catalytic converters, catalysts in industrial processes), biomedical applications (FeO_x-NPs as magnetic resonance imaging (MRI) contrast, site-directed drug delivery), food additives (TiO_x as white colour agent), and many more [Aitken 2006]. The amount of NPs being used is growing exponentially and some concerns have been raised as to their heavy use in regards to accumulation in the environment and health risks [Buzea 2007]. Analyses of product lifecycles have shown that they are accumulating and persistent in the environment [Gottschalk 2009].

Iron oxide nanoparticles (FeO_x-NPs)

Iron oxides are partly present in PM due to weather erosion of magmatic soils, but are for the most part a by-product from industrial and mechanical sources [Cornell 2003, Wahlström 2010, Linak 2007], thus it is often seen as a marker for anthropogenic activity [Furusjö 2006]. Iron oxide NPs are in reality a collection of different types of NPs depending on the crystalline phase of the iron oxide. The main synthetic iron oxide phases used for NPs are magnetite ($Fe[II,III]_3O_4$), hematite (α-$Fe[III]_2O_3$), and maghemite (γ-$Fe[III]_2O_3$). The most versatile iron oxide NPs are magnetite, which are stable and superparamagnetic and so have desirable properties if used for MRI-imaging in the form of (ultra small) superparamagnetic iron oxide nanoparticles

1. The novelty of commercial use. It is worth to point out that nanoparticles are naturally occuring being generated in aqueous solutions as nucleic precipitation of poorly soluble solid phases in *e.g.* ground water.

([U]SPIONs). SPIONs are sufficiently small that when ingested enter the body and are spread throughout and so act as a contrasting agent [Song 2011, Stephen 2011]. Although magnetite is mainly used, maghemite has a crystal structure akin to magnetite and the exact nature of the applied materials is often poorly understood. Moreover, the biological activity can potentially be dissimilar. Novel uses of magnetite NPs include drug applications where NPs are surface modified to carry a therapeutic agent, which are then guided to the wanted area of the body by magnets so that the release of the drug can act locally [Mahmoudi 2011]. This practice maximizes the effectiveness of the drug and minimizes the side-effects which most drugs induce. Iron oxides in general have found application in industrial catalysts, chemotherapy, electronics, pigments, and paints [Teja 2009].

Palladium nanoparticles (Pd-NPs)

Palladium is a transition metal from the platinum metal group (PMG) which includes Ru, Os, Rh, Ir, and Pt. It is scarce in the earth's crust and practically non-existent in the atmosphere, except for emissions from metal smelters and automobile catalytic converters [Glaister 2010, Rauch 2005:2]. More than 60% of mined Pd worldwide is used in catalytic converters [Ravindra 2004] most of which ends up in some form as pollution in the environment and additionally the amount of Pd in the environment has been shown to be accumulating [Rauch 2005:1, Limbeck 2007]. Pd is incorporated into a cordierite matrix (synthetic aluminosilicate ceramic) in catalytic converters usually in combination with Pt and Rh where it is deposited in NP form. The hollow cordierite structure means that exhaust gases are dissipated over the matrix with an active surface of about 80-3200 m^2/m^3 (depending on matrix material used). The matrix is heated to temperatures over 800 °C and the catalytic effect of the deposited metals reacts with the exhaust gas to I) oxidize any hydrocarbons to CO_2, and II) reduce any nitrous components into N_2 (producing H_2 as a by-product). The catalyst effect means up to 90% of gaseous emissions are transformed into inert species, but a problem exists in that particulates are not generally affected [Winterstein 1998, Acres 2004, Kaspar 2004]. Some vehicles, mostly diesel driven ones, have particle filters to remove PM emissions, however they are not wholly effective since ultrafine particles can still bypass the filters, including loss of catalytic material from catalytic converters [Goncalves 2008].

3.2 Monitoring and legislation

Monitoring of air pollutants is handled by national governments and mostly adhere to the guidelines set forth by the World Health Organization [WHO 2005]. Monitoring is mainly aimed at gases and PM that have been shown to cause adverse health effects [Dockery 1993]. Since the late 1970s the European Union (EU) has adopted the WHO recommendations and compiled both short- and long-term exposure limits, handled by the European Environment Agency (EEA) and the Sixth Community Environment Action Programme. The programme details, among other things, the aim in reduction of ambient PM, monitoring practices, future reduction targets, and enforcement of legislature. For a summary of the emission limits, see Table 2.

Table 2. *Table of the limit values set by EEA in 2008 for monitored air pollution in relation to protecting human health. DNA =Does Not Apply,* = daily 8-hour mean. [Directive 2008/50/EC]*

Pollutant	1 h average	24 h average	1 y average
SO_2	350 μg/m^3 not to be exceeded more than 24 times per year	125 μg/m^3 not to be exceeded more than three times per year	*DNA*
NO_2	200 μg/m^3 not to be exceeded more than 18 times per year	*DNA*	40 μg/m^3
PM_{10}	*DNA*	50 μg/m^3 not to be exceeded more than 35 times per year	40 μg/m^3
$PM_{2.5}$	*DNA*	*DNA*	25 μg/m^3
Lead	*DNA*	*DNA*	0.5 μg/m^3
Benzene	*DNA*	*DNA*	5 μg/m^3
CO	*DNA*	10 mg/m^{3,*}	*DNA*

Monitoring is done on the basis of a set mass per volume of air, i.e. usually μg/m^3, over a period of time. In relation to PM some inherent problems exist for this paradigm: while a mass-per-volume can be correlated to negative health effects it is a coarse view of exposure, that is, it does not take into account the individual particles and their chemistry. As will be detailed below depending on the size of the PM, structure, crystallinity, and/or surface chemistry different health effects are observed. In a general sense the model works but in order to detail local exposure and emission of PM must this fallacy be addressed. For now, no limits on ambient ultrafine PM exist. This is mostly because it is difficult to monitor them reliably and specialist instrumentation is needed. Ultrafine PM accounts only marginally mass-wise of the total PM, but they increase in number exponentially from 1 μm in size and below. Also, the surface area of these particles increases exponentially as

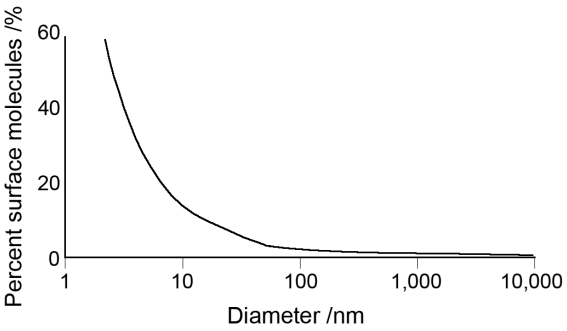

Figure 2. The percentage of particle surface as a function of particle size. The surface-% increases exponentially from approximately 100 nm and below. Image modified from Oberdörster *et al.* [Oberdörster 2005].

they get smaller if compared by a surface-to-bulk ratio as illustrated in Figure 2. This means that the surface chemistry of the particles starts to play a major role when the particles are of a sufficiently small size and so the chemical elements of the particle are important and any associated surface configurations [Monteiller 2007].

3.3 Health effects

Reports of the adverse health effects of PM began to appear in earnest in the 1970's. PM_{10} was deemed the main culprit for a long time, and it was soon discovered that $PM_{2.5}$ may have distinguished and separate effects from those seen for PM_{10}. Only recently has it been realized that particles, which are much smaller (<0.1 μm) than the main size mode of $PM_{2.5}$, also have a unique effect on the exposure host. The details of these specific size modes of particles and the way they are taken up at exposure and their effects are described below.

3.3.1 Modes of exposure

Vectors of exposure for PM can happen by a multitude of ways: Inhalation (primary), digestion (secondary), and absorption through the skin and the eyes (tertiary). Inhalation is by far the most common exposure route as PM enters the lungs through respiration. Depending on the size of PM, particles are effectively filtered by different regions of the lungs: PM_{10} is retained in the upper bronchial region and $PM_{2.5}$ is retained in the alveolar (gas exchange) region. Smaller sizes of PM are not filtered in the lungs and are deposited, more or less, homogenously throughout the lungs. Figure 3 is an illustration of the routes of exposure.

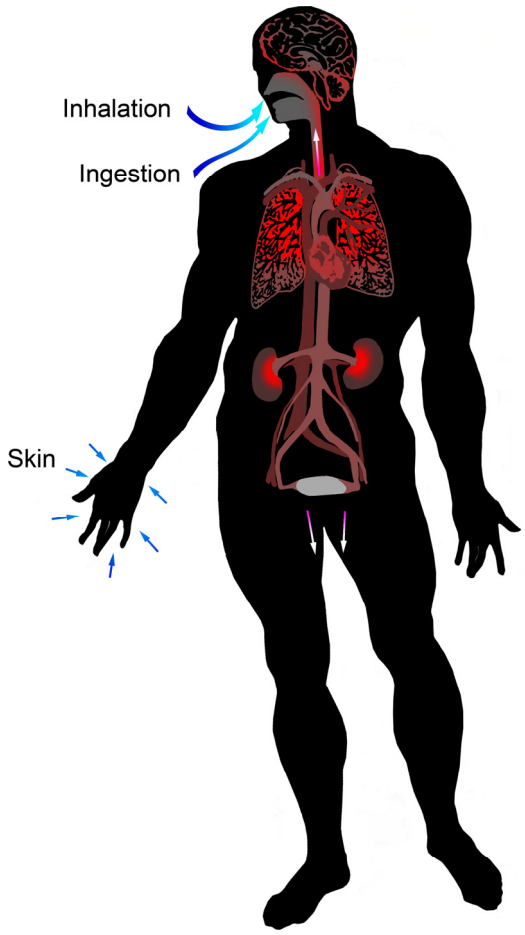

Figure 3. Illustration of the human body with an example of possibly affected organs from exposure to PM. Exposure routes are marked by blue arrows and clearance routes are marked by pink-white arrows. The red areas represent the areas at most risk from harmful PM.

3.3.2 Modes of action

PM that comes into contact with cells in the body can exert its toxicity either extra- or intracellularly. In order to be toxic on the inside of the cells the particles need to be taken up by the cell. This can happen either by kinetic forces (particulates wearing down the extracellular membrane or puncturing it by force), diffusion, or being admitted through the cell membrane [Apopa 2009, Andersson 2011]. Commonly micrometer sized particulates do not easily pass into cells and are brought there either as part of phagocytosis or cell damage [Zhu 2008]. NPs on the other hand are readily admitted into cells and pose a serious risk in this regard [Brandenberger 2010].

3.3.3 Bodily defences

When exposed to PM the body can take up a certain amount of particulates depending on the route of exposure. The skin is the body's most effective way of stopping PM absorption and is virtually impenetrable. If the skin is damaged or weakened then it is less effective. However there exists some concern that some NPs can be absorbed through the skin [Tsuji 2006]. Similarly PM entering through the digestive tract is subject to a rigorous chemistry and is for the most part dissolved. Although the immediate harm of PM is removed, certain dissolved chemical species can still be harmful [Golobič 2012].

PM entering the lungs represents the most aggressive form of exposure. While the lungs have certain mechanisms like cilia to filter out particles, PM_{10} and below are sufficiently small to bypass this filtering and are deposited in the lungs. PM_{10} is generally deposited in the bronchial region of the lungs while $PM_{2.5}$ is deposited in the alveolar region [Godoi 2008]. Some defensive measures still exist such as the mucociliary fluid film that coats the inside (epithelial cell layer) of the lungs. When deposited, PM can be trapped in this fluid and then be cleared by the upward motion of the fluid, by cilia, from the lungs to the trachea. Reports show that inhaled particulates are cleared in this manner, but a portion still remains [Katsnelson 2010]. The retained portion can be attacked by phagocytes which encapsulate the particulates to either be digested by host cells or effectively cleared through the mucociliary fluid [Krpetić 2010]. The remaining particulates that are not cleared, or not cleared fast enough, can act locally by leaching ions that disrupt essential biological processes, lead to the formation of reactive oxygen species (ROS), or cause mechanical damage.

Evidence suggests that PM can transgress into the blood stream and be distributed throughout the body, ending up being deposited in other organs (liver, kidneys) [Kreyling 2002]. When deposited in other organs they can again be chemically active at that location but can also be cleared by other means (renal clearance or defecation). It would seem as though the uptake into the blood stream is size-dependant, that is, the smaller the particle the more likely it is to pass over into the circulatory system [Nemmar 2002]. There are reports of NPs being able to transgress the blood-brain barrier, although this seems to be governed by the NP type rather than the size, although the small size is a prerequisite [Dziendzikowska 2012].

3.3.4 Adverse effects

Ambient concentrations of PM have been linked to acute, short-term, health effects from respiratory illnesses (allergies, asthma, respiratory infections) and to chronic, long-term, effects (cardiovascular disease, sensitization to allergens, mortality) [Walker Jr. 2008]. Often times the effects are not immediate, but cause an inflammatory response which can be measured [Lebowitz 1996, Park 2010]. Below is a summary based on the most recognized views on toxicology from particulates.

Size-dependent toxicity

Relating the toxicity of particles to size alone is unfortunately a complex issue due to the simultaneous toxicity stemming from the particle chemistry where the chemical influence is usually the strongest. Irrespective of this some

examples exist. The size-dependent toxicity comes into effect mainly for NPs, as their size can be small enough to inhibit biological activity by size alone.

Pan *et al.* have shown that Au-NPs of a specific size of 1.2 and 1.4 nm cause cell apoptosis and necrosis and are speculated to intercalate with DNA strands, disrupting their decoding during transcription, while smaller and larger NPs of the same material remained virtually non-toxic [Pan 2007]. Another aspect is that since the particles are small they can be incorporated into cells and exhibit their chemical toxicity there. For example, Karlsson *et al.* compared micro- and nanometer size particles of identical composition (CuO and FeO_x) and found that the NPs induced cell death and mitochondrial damage. Conversely they found the opposite effect for TiO_2, that the micrometer sized particles induced more toxicity than their NP counterpart, relating this effect to the crystal structure of the material [Karlsson 2009].

Going back in history there was the infamous example of asbestos exposure as a carcinogenic agent in lungs derived from their rod-like fibrous form. Recently an analogy to asbestos has been drawn for carbon nanotubes. Their inherently small size and fibre-like morphology means that they can mechanically pierce cells and essentially cause harm comparable to asbestos. While the material itself (essentially graphite) is inert, the shape and form of these nanomaterials is of concern [Donaldson 2010].

Chemistry-based toxicity

Particles that are in a bodily environment can be promoted by *e.g.* surface complexation or dissolution to release ionic species that disrupt biological processes by replacing natural ions that are needed for the process to give the, for the cell, vital outcome [Colombo 2008].

Another outcome is that the particle surface itself can be reactive. For example, ROS formation has been shown to be the primary toxic component of FeO_x-particles. For FeO_x-particles the ROS are generated through Fenton-like reactions (Figure 4) on the surfaces of particles and, keeping in mind that the surface-to-bulk ratio increases exponentially with decreasing size, is most evident with NPs. ROS leads to oxidative stress in cells disrupting the normal functions of the cell since resources have to be invested into countering these effects. If the cells ROS harvesting capabilities cannot cope then the cell will undergo apoptosis or become necrotic [Naqvi 2010]. ROS related effects are suspected of occurring for other particle types, but the mechanisms for their formation are not necessarily known [Syed 2013].

A further aspect of particle toxicity is opsonization, *i.e.* the adsorption of a bio-corona consisting of peptides, lipoic acids, and proteins onto the particle. This will cause the cell to identify the particles through their adsorbed surface

character, that is, the cell sees the particle as a native biological product and thus allows its entry into the cell where the particle can mete out its toxic effects [Cedervall 2007]. Similarly the surface characteristics of some particles may permit them to adsorb essential proteins from the cell cytoplasm reacting and incapacitating them and causing cell stress [Sun 2013].

The special semi-conducting properties of quantum dots have given rise to their use in dyes and electronics. The use of certain heavy metal elements in their synthesis causes these NPs to exhibit high toxicity originating from the leaching of heavy metals. They are of serious concern in relation to their negative health effects [Shao 2011].

The possibilities of toxicity for particles are endless and adamant research is being done to further our understanding of their effects but can be avoided *e.g.* by surface modification (for therapeutic use) [Häfell 2009].

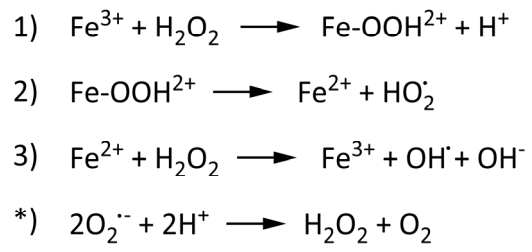

Figure 4. Modes of reactive oxygen species (ROS) formation from reactions with iron oxides in aqueous solutions as described by Zelmanov and Semiat [Zelmanov 2008].

3.3.5 Positive effects

Reports have shown that certain particulates can be beneficial in small amounts. The formation of ROS is a natural by-product of biological processes in the body. The chemistry of certain NPs such as Pd-NPs is that of ROS-scavenger. They can effectively harvest formed ROS species and react with them and thus lessen their impact [Kim 2008, Hikosaka 2008]. Their therapeutic use has been proposed, but remains questionable in that the particles themselves seem to still be harmful.

Novel ways of coating particles with therapeutic surface species to allow *e.g.* only cancerous cells to admit them to pass the cell membrane and enter into the cytosol, where the particle can act harmfully. This can be employed in a chemotherapy function, effectively using the harm from particles for good [Card 2008].

4 Experimental

There exist countless methods and techniques for the preparation, analysis, and characterization of particulates and testing of their effects on biological matter. This section presents some of the different methods and techniques and goes into detail regarding the methods used during the research for this thesis.

4.1 Particulate matter collection and analysis

The collection of particles for analysis is not a trivial matter. Usually particles are collected onto a substrate material such as a filter and then analyzed off-line, while on-line methods exist but are tricky to use routinely. Off-line collection is routinely done by cascade impactors where particles are separated by inertia from a pressurized (air) gas stream and partitioned according to pre-set size-modes [CARB 1990]. The particle fractions are then separately analyzed by different methods, see below.

Depending on the type of particles one is set on analyzing different techniques can be used to this end. As mentioned in the background section air pollution is a complex mixture of substances and chemical phases. Different information for the pollution can be obtained: size-modes, number of particles, crystal phase, and elemental analysis. For analysis of gases and VOCs established methods of analysis include gas chromatography (GC), mass spectrometry (MS), Raman or infrared (IR) spectroscopy, and flame absorption atomic- or inductively coupled plasma spectroscopy (FAAS /ICP) [Potgeieter-Vermaak 2012, Li 2013, Pillay 2012]. Complete analysis of aerosols on the other hand is not as straight forward and potentially requires complements of techniques for successful analysis. For example, X-ray fluorescence spectroscopy could be used to determine the elemental constituents of PM while GC/MS could be used to determine any gaseous species present [Prather

1994]. Detailed below are some useful techniques that were used in the research for this thesis and that have proven to be robust and versatile.

4.1.1 Custom particle entrapment equipment

A novel way of collecting particles was devised together with Sempore AB. It consisted of a battery driven air-suction unit on which filter stubs can be mounted. The unit has a flow-through volume of 1.5 l/h effectively capturing particulates with enough separation as to not cause overlap between individual particles during normal use.

Nucleopore filters

Nucleopore filters consist of a polycarbonate matrix that is interspersed by holes caused by radiation bombardment. Practically speaking it is a polymer film with uniform holes through which air can be sucked and any particles that are bigger than the pores get deposited on the film. The pore sizes of the filter and their number per area can be varied depending on the radiation used to bombard the filter. Figure 5 shows the filter surface of a typical nucleopore filter with pores. These filters were placed in special filter stubs consisting of a flat area with a hole in the middle through which the air could flow freely. The stubs were designed for easy use in scanning electron microscopes (SEMs) with no particular sample preparation needed for imaging.

4.1.2 Light scattering particle counter

Light scattering particle counters are used to determine the number of particles per unit volume of air, or to extrapolate the mass per volume. In essence a light scattering counter works by sucking air through a measuring cell to which a

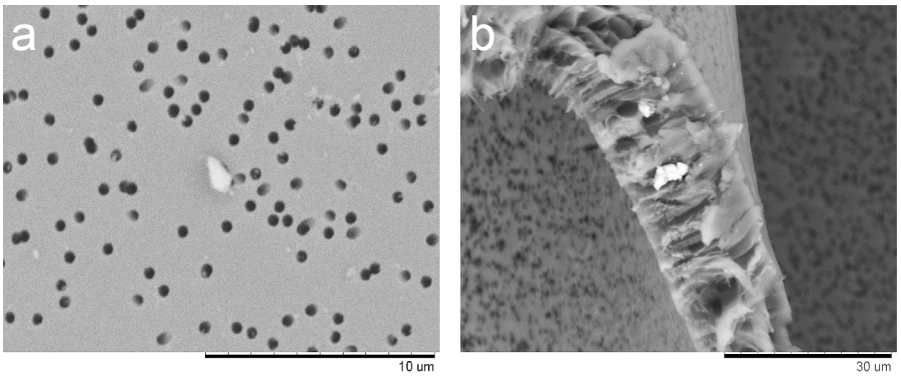

Figure 5. a) Slide shows a nucleopore filter with 0.5 μm pores; b) a rip in the filter shows the thickness of the substrate, which is approximately 20 μm thick.

laser diode is placed perpendicularly. The light from the laser diode crosses the gas stream and when disrupted causes the light to scatter at an angle depending on the refractive index of the causant particle, *i.e.* it scatters in a way deferred by the size of the disrupting particulate. The instrument used in this thesis was a Climet CI500-EC, which has channels to measure 0.3-0.5 μm, 0.5-1.0 μm, 1.0-5.0 μm, 5.0-10.0 μm, 10.0-25.0 μm, and 25+ μm. To this device it was sometimes necessary to fit a flow splitting air diluter. An Air Techniques TDA-D100 Aerosol Diluter (1:100) was used and in practical terms meant that 1/100th of the particulates was measured, keeping the sensitivity of the instrument at optimum and not causing too much dead time when measuring. The instrument was factory calibrated by polystyrene sphere standards.

4.1.3 Scanning electron microscopy, SEM

Electron microscopy uses electrons, instead of photons, to 'see' a sample. The SEM has a resolution that is several orders of magnitude better than light microscopes due to the (de Broglie) wavelength of the electrons can be made much smaller without diffraction

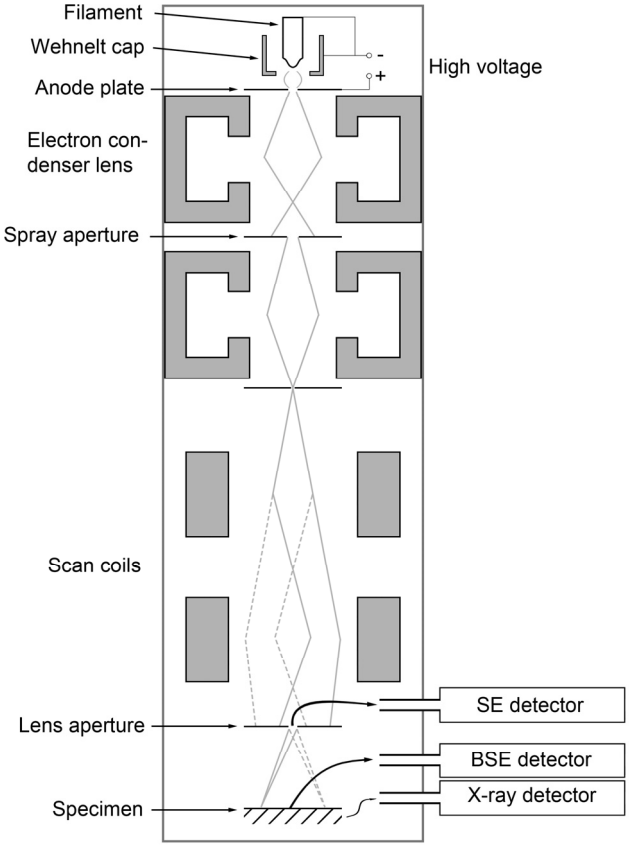

Figure 6. Illustration of a typical electron microscope column. A high voltage potential is applied over the filament causing electrons to escape the filament substrate. They are then accelerated by the anode plate to high speeds. The electron beam is then collimated by condenser lenses and homogenated by apertures. The scanning coils then direct the beam to raster scan the specimen. Radiation emanating from the specimen surface (electrons and X-rays) are detected by their respective detectors producing the electron micrograph image (and elemental analysis). SE = secondary electron and BSE = backscatter electron.

effects. The integral part of the electron microscope is the electron column, consisting of an electron gun and two or more electron lenses that collimate the electron beam to raster over the sample. A vacuum is applied over the electron column and sample. The most commonly used thermionic electron guns have usually a filament of W or LaB_6 which is charged with an applied electric field. When sufficient tension in the filament builds up, the electrons exit the filament material and exist for a short period beyond it. Another electric field around the mouthpiece of the gun accelerates the electrons downwards in the electron column and the electrons gain energy between 0.2-40,000 keV. Condenser lenses then act to collimate the beam, producing a highly coherent and homogenous electron beam. The beam finally enters the scanning coils which direct the beam to raster-scan the specimen surface [Goldstein 2007]. For a summary and visual representation see Figure 6.

The beam itself, depending on the instrument and voltage used, has a spot diameter of 0.4-5 nm on the specimen surface and interacts to a depth of approximately 1 μm of the specimen (Figure 7a). Imaging quality is dependent on the achieved probe current on the surface. When the electrons enter the specimen material they interact with the atoms there, since the positively charged atom nuclei are more localized and denser in charge than the negatively charged electrons. Two types of electron scattering occur: elastic (electron is deflected but loses no kinetic energy) and inelastic (electron loses kinetic energy to specimen atoms).

Elastic scattering causes the electrons to be deflected laterally and if deflected enough times may turn around and leave the specimen causing

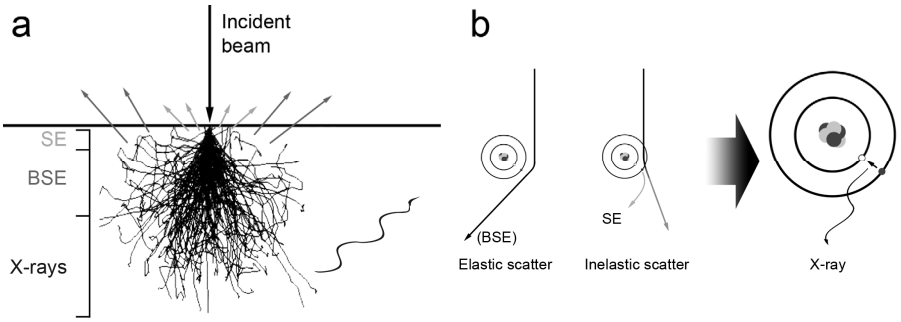

Figure 7. a) Schematic representation of the interaction of the incident electron beam on the specimen surface with marked paths of electrons and radiation regions. b) Elastic scatter gives rise to backscattered electrons (BSE) by non-kinetic deflection while inelastic scatter causes a disruption in the electron shell of the atom ejecting a secondary electron (SE). The vacancy in the inner core shell electron will be substituted by another electron from an adjacent shell and the energy difference emitted as an X-ray photon.

backscattered electrons (BSE). The chance of backscatter is greatly influenced by the atomic number of the specimen atoms, *i.e.* higher atomic number causes more backscatter (Figure 7b). This is important when imaging as using a BSE detector for imaging gives topographical information of the specimen surface and an intensity gradation depending on the atomic number of the specimen atoms.

When inelastic scattering occurs, the electrons interact with the specimen atom electrons, transferring kinetic energy from their motion over to the atom shell electrons and losing speed. This transfer of energy causes the atom electron to be excited to a higher energy level, and if the level is sufficiently high the electron may leave the host atom casing a secondary electron (SE) emission. The SEs then scatter through the specimen and can be detected by a SE detector.

Recent advances in miniaturization of electronics have led to the development of smaller and more compact SEMs. The new tabletop variants as made by *e.g.* Hitachi (TM-3000) and Jeol (JCM-6000 Neoscope) are so called because they fit on top of a standard workbench. They are usually somewhat limited in their capacity (no control of beam by software or fixed gun voltage and probe current), but offer comparable resolution of imaging to conventional SEMs. Above all they are usually easy to use and so are suitable for untrained professionals and afford the possibility of detailed chemical monitoring of PM.

Energy dispersive spectroscopy, EDS

Through inelastic scattering vacancies in the specimen atom electron shells are created as electrons are ejected. An electron that is in a higher and adjacent shell will relax down in shell order to replace the vacancy, losing some of its inherent energy in the process. This difference in energy is released as a photon emission having the specific energy difference between the shells and is in most cases of sufficiently high energy to produce X-rays. What this means is that since the shell configurations for all elements follow a very strict energy order so detecting the energy of the produced photons allows elemental classification of the parent atom. This is a very important and useful tool as qualitative information of the atomic content of the specimen can thus be obtained. Also possible is the quantification of the elements in the sample as the amount of X-ray radiation produced can be related to the amount of atoms present. Although certain atoms are more easily ionized in this process, calibration against standards removes most inferred error.

Traditionally liquid N_2 is needed to cool the single-crystal detector of an EDS, but are being replaced by a new line of silicon drift detectors (SDD). SDD detectors are piezo-electrically cooled by a Peltier element, and offer a

higher X-ray detection capacity than the single-crystal detectors despite operating at temperatures of approximately -40 °C (as opposed to -200 °C for N_2-cooling). This removes some of the maintenance need of conventional SEMs and ensures that a tabletop SEM can be run by power from the regular household electric output grid. This revolutionary improvement was pioneered by, among others, Bruker Nanolab Technologies that produced the Quantax detector series.

Automated analysis

Most conventional SEMs have software controlled interfaces where the beam voltage, probe current, and rastering can be controlled by computer. This offers the advantage of programmability to SEM analysis. By manually or by programming the software it can be made to scan the specimen and detect any inclusions or particles present in the specimen substrate and sequentially perform elemental spot analysis on these inclusions. By automated analysis large amounts of information on the samples' elemental constituents can be gained saving both time and effort and making routine analysis methods possible.

Elemental mapping

Another feature of most SEMs fitted with EDS is the possibility of using EDS in conjunction with imaging. The signals produced from the specimen can be detected by several detectors at once and so elemental information on the specimen can be related to *e.g.* the BSE-image of the same. This method can be time-consuming and some imaging resolution is lost since the EDS-information generally has lower resolution than the BSE and SE counterparts. But detailed information can still be gained of the elemental distribution of a sample, divided channel-wise by element.

4.2 Statistical methods

Statistics offer useful tools for analysis, interpretation, and presentation of data. Explaining if there is a deviance to an expected result and quantifying the deviance are a matter of choosing the right statistical methods and applying them correctly. Of course there can be bias as there are really no 'correct' methods, but rationalizing the method selection ensures that some credibility is afforded to the results. In science theory, adopting a hypothesis and then testing the null hypothesis by statistical means is common. If deviation from the null hypothesis is evident as shown by the mathematical model adopted in

the statistics test then support can be asserted for the hypothesis to be correct, although it must not be, as formulation of the hypothesis can be tricky.

4.2.1 Analysis of variance, ANOVA

ANOVA is a statistical method for testing hypotheses, that is, by applying the method to data a measure of deviance (p, probability-value) from the normal distribution is obtained. Depending on the nature of the data (number of categories, datapoints, degrees of freedom) a calculated F-value is compared to tabulated data. If the F-value is higher than the threshold value it can be ascertained by a measure of certainty that the data deviates from normal distribution, *i.e.* the results are not explained as happening by pure chance.

The strength and robustness of ANOVA as a method for cross-testing multiple variances stems from its' simple design. For i groups of data containing N_i data values a group mean, μ_i, sum of squares, SS_i, error of the SS_i (SS_{error}), and SS for among groups, SS_{among}, are calculated. For a general prediction, the parameter F is calculated (Eq. 1):

$$F = \frac{SS_{among} / df_{among}}{SS_{error} / df_{error}} \qquad \text{(Eq. 1)}$$

where df is the degrees of freedom for the 'among' (i-1) and 'error' (N-1) sum of squares respectively. If the F-value is greater than the tabulated value then a significant result can be deduced. Commonly a least significant difference, LSD, is calculated by calculating confidence limits, determined by the level of confidence one wants to test, *e.g.* 95% confidence, (Eq. 2):

$$LSD = t_{N-1} \bullet \sqrt{\frac{2}{n} \bullet \frac{SS_{error}}{df_{error}}} \qquad \text{(Eq. 2)}$$

where t_{N-1} is the tabulated threshold value for the selected confidence interval [Barnard 2001].

4.2.2 Principal component analysis, PCA

Some data sets can quickly become too large to handle by simpler linear univariate statistical models due to the number of variables that are influencing the outcome variable. PCA is the most used multivariate model for detailing complex data structures in an efficient manner. It works by deconstructing a data matrix, consisting of n objects and p variables ($n \bullet p$ matrix), into two

separate matrices, *X* (structure matrix) and *Y* (noise matrix), that is, *X* is the PC-model and *Y* is the error of the model (to the real data).

By deconstructing a data matrix three objects are calculated: PC score matrix *T*, the loadings matrix *P*, and the error *E* (noise or lack of fit) through the NIPALS (non-linear iterative projections by alternating least-squares) algorithm [Esbensen 2002]. The model can be described as a matrix product (Eq. 3):

$$X = TP^T + E \qquad \text{(Eq. 3)}$$

where P^T means the *P*-matrix is transposed. Since the variance of the model can be constituted of several different phenomena, each being described by different variables, many PCs can be calculated (up to *n* or *p* in number). Indeed it often times is necessary to describe a multivariate data set by several PCs as that is the point of using it! The first PC should describe the majority of the models' variance and each subsequent iteration of the NIPALS-algorithm should produce a new PC with a lower degree of variance explanation. For each repetition a new *t*, *p*, and *e* matrix is calculated describing some of the rest of the variance carried over by the preceding steps error. Figure 8 illustrates this procedure.

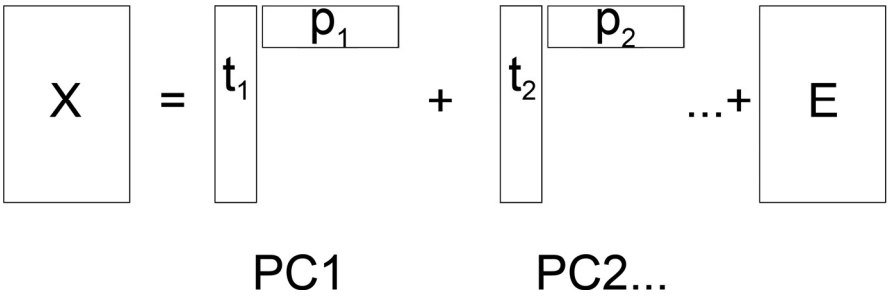

Figure 8. The PC-model X is the sum of the vector product of the t_i, p_i, and E vectors/matrices. Each individual PC describes a part of the total model.

The advantage of using PCA modeling is not only that multiple variables can be handled at once, but also the intuitive visualization it offers for the data. Instead of viewing the data from an orthogonal point of view where maybe 2-3 variables can be handled at the same time, PCA allows the visualization of the data in *n*-dimensional space. When the PCs are calculated they represent some trend that explains the data, the PC axis. A plot can then be made for each data point as a projection of the least squares fit to the PC axis. As the value is squared, the more it deviates from the PC axis, the more it influences the PC. Multidimensional space can be hard to understand, but as most models contain

their description in the first few PCs the information can be displayed in two dimension through the projection of the data on the plane between the two PC-vectors thus giving information on two PCs at the same time, or more if more dimensions are desired.

4.3 Engineered nanomaterials

Nanomaterials have been synthesized (unknowingly at the time) since antiquity mainly for colouring pigments, *e.g.* for staining of glass. Recently engineered nanomaterials have found novel uses in commercial products and research items exacerbating the need for well defined materials with specific functions. There are two basic approaches to the synthesis of engineered nanomaterials or NPs: the top-down and the bottom-up approach.

The top-down approach is concerned with taking a substrate material and deconstructing it into ever smaller units until the desired material is obtained. For example milling a hard material into fine dust can produce NPs [Mohammednezhad 2012]. Other techniques include laser ablation, lithography and focused ion beam (FIB) milling [Liu 1996, Xu 2007], and atomic layer deposition (ALD) [Bangert 1996]. The main drawback of using these methods is that the properties for the produced particulates are largely governed by the bulk material and any modification to make them suitable in different environs needs to be done *post synthesis*.

The bottom-up approach on the other hand is concerned with assembling smaller units (like molecules) into larger units until arriving at the desired size of the nanomaterial. This approach affords more options since the methods generally are performed in step-wise fashion and can be added to or modified during the steps to incorporate other materials making complex structures of nanomaterials [Riehemann 2009]. Often times the size and morphology of the produced material, together with the surface charge and magnetic properties, can be controlled by adoption of different reaction media [Li 2010, Pazik 2009]. Examples include nucleation of gas or liquid/gas, precipitation from dissolved precursors (sol-gel, thermal decomposition, pH-aided, electrochemical, microemulsion, hydrothermal), and polycondensation of self-organized micelles [Neyshtadt 2008, Fadeel 2012, Venkatesh 2013].

4.3.1 Synthesis of Fe_3O_4-NPs

When specific custom-tailored NPs are needed for use the method of choice of procuring them are solvation based. Methods based on aqueous and non-aqueous chemistry are available and the choice usually comes down to the specific properties the NPs are desired to possess. The added advantage of

using a chemistry based route of synthesis is reproducibility, control of parameters for tailoring the NPs and furthermore cost-effectiveness and up-scalability. All chemical methods share the same principles: dissolution of a salt or precursor material and the subsequent chemical reduction to precipitate particulates, only differing in use of solvent, reaction environment (heating, pH, pressure, atmosphere), and an eventual addition of surfactants for co-precipitation.

Aqueous synthesis is a fairly simple procedure in that a salt is dissolved in an aqueous solution. The NPs can then be precipitated by mediation of pH, addition of a co-precipitant, or electrochemically causing the reduction of the solved ions in favour of oxidation of the water. A surfactant can be applied to give a well dispersed colloidal solution. The process can be done under high temperature and pressure (the hydrothermal method)

Non-aqueous synthesis follows the nucleation of the iron oxide NPs through reaction in an organic medium. Hydrolytic reactions use iron chlorates or iron alkoxides as a precursor. When water is added the water acts as an acid in the organic solvent and hydrolyses the precursor leading to nucleation of the conjugate iron from the precursor. As oxygen from the water or alkoxide is retained by the conjugate the nucleation formation results in an iron oxide moiety. These then aggregate to form NPs. The aggregation governs the size of the produced NPs and usually is halted as the surface charge is distributed over a wider area lessening the nucleation reaction and increasing the interaction with the reaction medium (solvation) leading to a reaction equilibrium.

The iron oxide NPs used for the research in this thesis were formed in a non-hydrolytic manner by dissolving iron(III)acetylacetonate ($Fe(acac)_3$) in acetophenone ($C_6H_5C(O)CH_3$) and refluxing at the solvent boiling point (202 °C) for a specific time.

4.3.2 Synthesis of metallic Pd-NPs and Pd/Al-nanocomposites

Palladium being a noble metal reacts slightly differently from iron and forms mostly metallic particles and rarely oxides. In aqueous solutions the procedure is straightforward as a dissolved salt (or acid dissolved metal) can be precipitated by a reducing agent *e.g.* sodium borohydride ($NaBH_4$). In organic solvents (*e.g.* xylene or acetophenone) the need for a reducing agent is eliminated as the reaction media itself can act as the reducing agent by complexation of the solved ions via thermal decomposition. Both methods produce metallic NPs.

Nanocomposites are composite (multi-phase mixture) materials, where at least one component is present in nano form. In case of noble metal catalysts, produced commercially as a deposit of NPs on a cordierite (aluminosilicate)

carrier matrix, it was necessary to model composite NPs containing Pd together with aluminium oxide.

For this thesis metallic Pd-NPs were produced by dissolving palladium(II)acetylacetonate ($Pd(acac)_2$) in acetophenone. Pd/Al_2O_3-nanocomposites were formed by simultaneous decomposition of $Pd(acac)_2$ together with $Al(O^iPr)_3$ in acetophenone resulting in about 12 nm sized Pd-NPs incorporated in a matrix of smaller 2-3 nm Al_2O_3-NPs.

4.4 Characterization of nanoparticles

To be sure of the results being reported from the effects of NPs it is important that as much information about the NPs is available as possible for reproducing the results. As is the case many times reports of one effect for one set type of NPs may or may not occur for similar, yet slightly modified particles of the same type. Physicochemical factors that come into play are size (diameter, volume), morphology (spherical, plates, rods, fibrils *etc*.), crystallinity (crystal phases, amorphousness, porosity, defects), and surface configuration (adsorbed species, oxidised surface layer, surface similarity to bulk). As most use of NPs is in some kind of solution the NP properties in the solution are vital. Do the NPs disperse or agglomerate/aggregate, what is the hydrodynamic sphere like, what are their surface charge, are they dissolved, do they possess a magnetic momentum, are all essential questions to be addressed before a study. To this end there are a whole host of techniques one can delve into and often times no one technique can address all issues. Rather they are complementary and using several different types of techniques ensures that a complete picture of the NPs properties can be approached.

4.4.1 Transmission electron microscopy, TEM

TEMs generally have several orders of magnitude better imaging resolution compared to SEMs as the principle of electron detection is different, although the principle of the electron column is very similar. Electrons that enter the specimen are transmitted through it and collected on the bottom below the specimen. As electrons are transmitted through the specimen some may be absorbed and so are lost and not detected, a process which is heightened by the samples atom thickness. Thus an image appears of the sample where atomically dense regions appear darker than the less dense regions [Williams 2009]. Since the electron transmission is inversely dependent on the thickness of the sample only very thin samples may be imaged somewhat limiting the use of TEM, see Figure 9 for an illustration of TEM functions. TEM offers a very powerful magnification where individual columns of atoms can be seen if

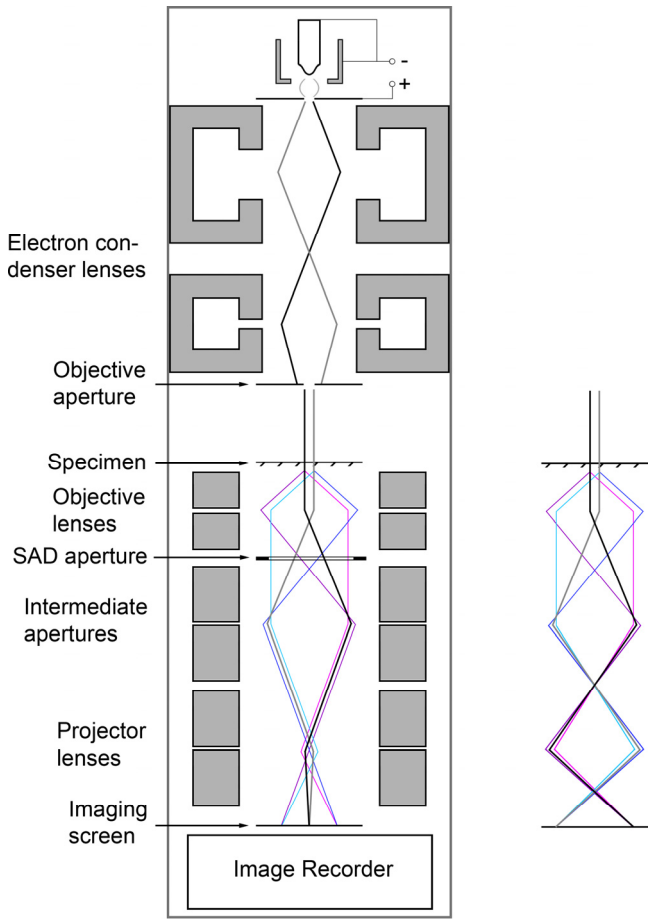

Figure 9. Transmission electron microscope (TEM) column. Many features are similar to that of the SEM (Figure 6) although the main difference being that electron are transmitted through the thin sample and detected from below. Two different ways of gaining information from a sample are (*left*) selected area diffraction (SAD) where a diffraction pattern for the sample can be obtained and (*right*) imaging producing an electrograph of the specimen.

the crystal structure is oriented in the correct way. Generally samples are deposited on 3 mm diameter copper grids with a thin layer plastic film and then inserted into the TEM. This is a very useful way of imaging the sizes and morphology of NPs.

Selected area diffraction, SAD

If the back focal plane rather than the imaging plane is set on the back CCD camera a diffraction pattern emerges as electrons are diffracted by the crystal structure of the sample. The specimens' space group symmetry can be read from this diffraction pattern much the same way as from X-ray diffraction, with possibly some orientation of the specimen.

4.4.2 X-ray powder diffraction, XPD

X-ray diffraction is the most used method of determining the atomic (crystal) structure of metals and organic molecules. A sample is mounted onto a rotating goniometer and illuminated by a focused X-ray beam. The X-rays transmit

through the sample as waves and as they traverse through the specimens' regularly structured crystal matrix they are reflected by the specimens' atoms (more specifically the electrons) causing a diffraction pattern to emerge. Although most of the emanating waves cancel out each other through destructive interference, according to Braggs' Law (Figure 10 and Eq. 4) certain reflections, that are in phase due to the spacing of the uniform crystal lattice, add to one another through constructive interference producing a diffraction pattern that is detectable by a CCD camera [Zou 2011]:

$$2d \sin\theta = n\lambda \qquad \text{(Eq. 4)}$$

Where d is the interplanar spacing, θ is the scattering angle, λ is the X-ray wavelength, and n is a multiple of the wavelength. From these reflections clear indices for the scattering angle are obtained, and when the angles for the reflections are deconvoluted, give the distances between atoms in the crystal lattice. By calculation or by referring to standards and tables the crystal phase of the sample can be determined.

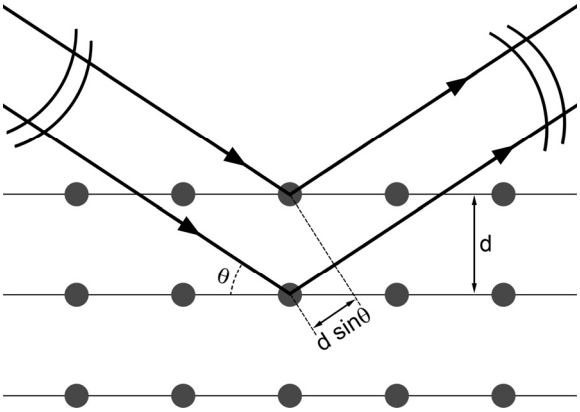

Figure 10. X-rays and electrons are scattered by the electron shells of atoms (grey spheres). As the incident radiation hits an atom it is reflected. As the atoms (in a crystal) are ordered in lattice planes the emitted reflections are in phase and an interference pattern emerges. θ = scattering angle and d = interplanar spacing.

4.4.3 Nanoparticle tracking analysis, NTA

NTA is done by injecting a sample into a quartz photocell where a laser illuminates the sample from the side. When the light hits the particulates in the sample it is scattered and can be detected by a light microscope with a CCD camera. The sample is filmed for a set amount of time and the movement from the detected particles are tracked by computer software. The particle movement is wholly accounted for by Brownian motion and is dependent on the size of the particle, *i.e.* the size if the particle is inferred from its diffusion movement in the liquid. The method is useful in that the only variables that affect the movement of the particles are the liquid temperature and viscosity and no consideration is needed for the particles refractive index. NTA is

sensitive in that particles from 10-1000 nm can be tracked. Also, information is gained particle-by-particle and so accounts for a true estimate of particulate sizes [Filipe 2010].

4.4.4 Dynamic light scattering, DLS

DLS is a useful method of obtaining the size-distribution profile of particles suspended in a solution. Similarly to NTA, a sample in a quartz photocell is illuminated by a (laser) light source. The light is scattered by the particulates in the suspension and as they are constantly in Brownian motion, the scattered light forms patterns with constructive and destructive interference (the scattering particle is moving around). Information on the size of the particle is thus contained in the dynamic interference pattern that emerges from the sample. This method provides a general profile of the sample interpreted from the sample interference pattern and is subject to some bias as a refractive index for the sample needs to be known beforehand [Pecora 2000].

4.4.5 Nuclear magnetic resonance, NMR

In chemistry there exist a few methods for structure determination, however, NMR presents a versatile, sensitive, and robust way of determining the structure of complex molecules and in addition can give information on intramolecular interactions. In short, a sample probe is subjected to a strong magnetic field from a superconducting electromagnet. The non-zero net quantum spin of an atoms nucleus, resulting from an odd nuclide (neutron/proton distribution), gives a magnetic moment that can be made to resonate by a magnetic pulse from the magnet. The resonance frequency pattern can be detected and deconvoluted using Fourier transform (FT). The resonance from a molecules atoms is dependent on their inherent magnetic moment but also dependent on interference from other atoms and functional groups. Thus the molecules structure can be inferred from the FT spectra of, for example the commonly used ^{1}H, relating their placement within the molecule and with respect to each other [Williams 1995].

4.4.6 Raman spectroscopy

Raman spectroscopy makes use of the inelastic light scattering that occurs when a sample in a quartz cell is illuminated by light. As the light interacts with the molecules in the sample it is up- and down-shifted by the related energy levels corresponding to the molecules vibrational modes. These can then be inferred from the resulting Raman spectrum that is obtained from the measurement and information on the properties of the molecule is thus gathered.

4.5 Air-way models for health studies

To assess the risks related to particulate exposure it is important to procure data from testing on live cells or living tissue. There is an inherent difficulty in gaining useful data for whole organisms as the effects they cause can be obscure which is why model systems are usually adopted to show specific effects. In the work for this thesis air-way models were used to show the effects of certain nanoparticles, and that is the focus for this section. The same methods can be used to show the effects of PM [Donaldson 2009].

4.5.1 *In vivo* testing

For the most part mice and rats are used as models for particulate exposure testing as their reactions to exposure correspond fairly well with how the human reaction would be [Geiser 2010]. Human testing is often times more expensive and can be ethically difficult which is why animal testing is chosen. Additionally since the metabolic pathways are much more accelerated in rats the effects are usually more clear and can be ascertained more surely than with human testing. Certain ethical criteria have still to be met to be allowed for testing.

Usually tests are performed either by normal inhalation or instillation (straight into the lungs) of particulate material. Other methods include ingestion through feed or injection of particulate material into specific parts of the animal [Poland 2008, Kim 2009].

The interesting effects to monitor in the lab animals concern mainly mutation and cancerogenicity, cell damage [Totsuka 2009], distribution of particulates in the body [Feng 2011], release of inflammatory biomarkers, production of ROS species [Könczöl 2011], and effect on lifespan [Kim 2008]. Any information gained in this manner is helpful in puzzling together the complex effects particulates may have and provide a clearer course for risk assessment.

Tissue testing

Live tissue and organs can sometimes be harvested from euthanized animals and kept living *ex vivo*. Some tests can be particularly toxic so ethical dilemmas may be the cause for extracting the tissue from the animal as not to subject the animal to particularly harsh treatment. Other times it may be interesting to study effects on just a certain organ, removing any befuddling effects that could be caused by other organs or by the cardiovascular system.

Examples include removing major organs like lungs, brains, kidneys, spleen, and liver for testing [Singh 2013].

4.5.2 *In vitro* testing

In vitro testing usually foregoes any ethical questions by the harvestation of cells from animals for out of body testing. Specific effects can thus be linked to a certain particulate in a cellular environment. Also it can be used to investigate the details of any uptake effects of particulates into cells, cell/particulate interactions [Witasp 2009], and dissolution effects of ions from particulates [Larner 2012].

Primary cells

Extraction of live cells from living organisms are denoted as primary cells. These cells can be cultivated in vitro, but do grow old and will die after a time. Extraction examples include harvesting from euthanized animals through bronchoalveolar lavage (BAL) to obtain certain cell types for testing. The advantage of using primary cells is their close representation of the tissue cells that particulates might affect and so are an important tool for estimating the real effects from particulates.

Cancer cells

For routine analysis primary cells may be hard to procure in sufficient quantities or be too expensive. A catalogue of transformed cancerous immortalized cells exists. The advantage of using this type of cells is that any results obtained from them are reproducible since they have been standardized, stemming from the same source. As they have been used extensively results between studies can be compared and they are not subject to differences from the individual source organism. Also in comparison to primary cells, they are more robust and less prone to infections making them easier to work with.

Air-lift models

Recently air-lift models have been realized and started finding their way into cytotoxicity studies. Air-lift models are an attempt at *post hoc in vitro* reconstruction of tissue from cultured cells [Yoshida 2011]. This is done as an attempt to side step the need for living tissue and unnecessary euthanization of animals. This model holds promise for future toxicity testing of particulates, but is still largely being developed.

5 Results and Discussion

5.1 Collection, analysis, and source apportionment of PM (papers I and II)

Two studies were conducted where PM was captured on nucleopore filters and subsequentially analyzed using SEM-EDS. The first study (paper I) was performed in order to show that the collection method was feasible and that not only could elemental analysis be used to discern the elemental constituents from individual particles, but also that the origin of the particles could be rationalized. In the second study (paper II) particles were captured in and around a heavily utilized roundabout at distinct points in time. The elemental constituents of the particles were investigated using automated SEM-EDS analysis and the data was inspected through means of statistical analyses to show the prevalence of particle types with time- and space resolution.

5.1.1 Collection of PM

As detailed in the background section, some difficulties in monitoring airborne PM exist, namely that no regard is taken to the chemical nature of the individual particulates. To address this, a study was undertaken where PM was collected at key points in- and around the city of Uppsala. Uppsala represents the fourth largest city in Sweden with a population of approximately 200,000. The collection points were determined so that I) a rural background, II) an industrial area, and III) inner city were represented for contrast. (Figure 11, circled numbers).

For the second study it was important to show that as the collection and analysis were feasible, to up-scale the procedure by collecting particles and by-passing the time-consuming manual analysis of the particles via automated analysis. For this study a heavily utilized traffic roundabout was selected as the

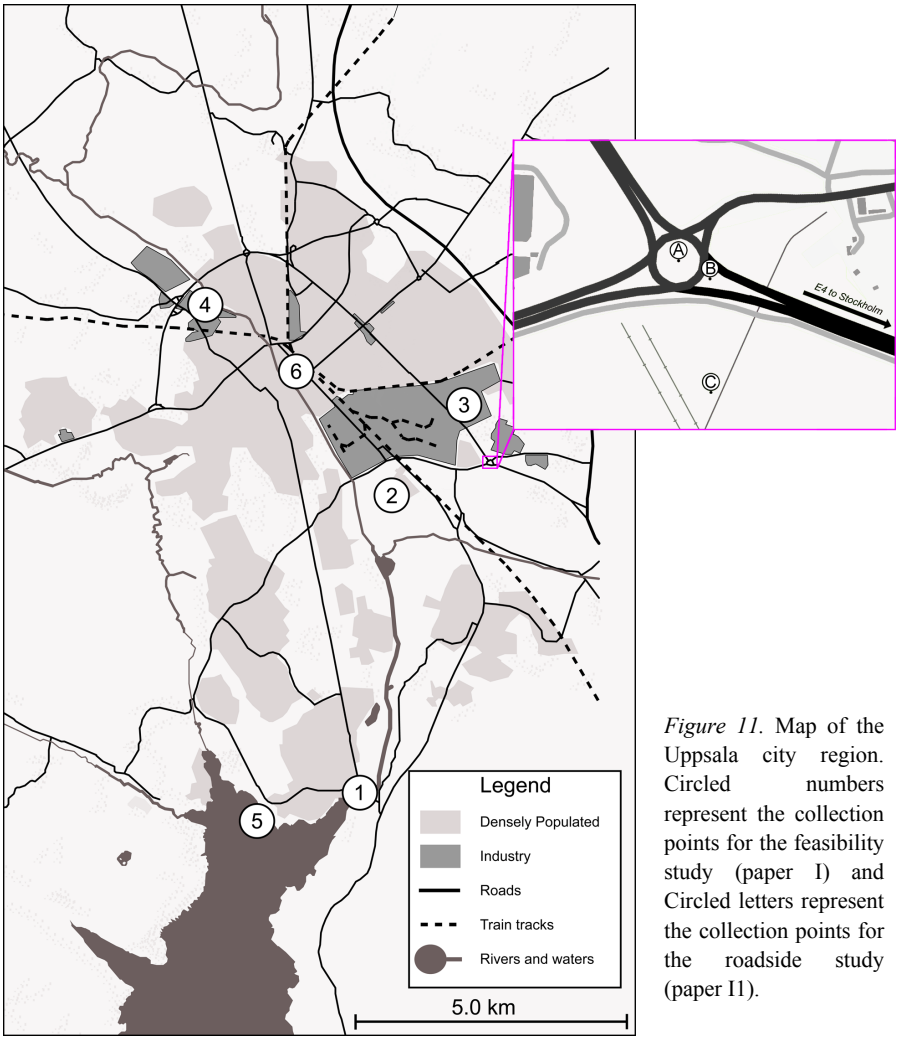

Figure 11. Map of the Uppsala city region. Circled numbers represent the collection points for the feasibility study (paper I) and Circled letters represent the collection points for the roadside study (paper I1).

collection area. Three points were determined at this roundabout: A) mid roundabout, B) roadside, and C) rural background (Figure 11, circled letters). The roundabout serves as an interesting subject as it is the main connection point for the E4 motorway between Uppsala and Stockholm and it was thought that cars entering the roundabout from the direction of the motorway would need to lose speed to safely maneuver through the roundabout. This loss of speed, predominantly caused by braking, should reasonably cause emissions from brake wearing. To fully put the analysis method to the test the standpoint was taken that a difference in occurring particles with high iron content could be correlated with point of collection (proximity to road) and collection time (heavy- vs. light traffic). For each of the three collection points four time

points for collection were determined to cover the main traffic episodes: 10 am, 12 am, 2 pm, and 4 pm. Concurrently with the collection of particles, for each collection a light scattering particle counter was employed to provide data of the total amount of particles in the air for each collection.

5.1.2 Analysis

Analysis of the particles caught on the nucleopore filters in the first study was done using a Hitachi TM-1000 SEM-EDS and in the second study using a Hitachi S-3700 SEM-EDS. Analysis was done particle by particle by first imaging the analyzed particle and then focusing the electron beam on said particle for the EDS analysis. For both instruments chemical information for each individual particle was obtained.

Measuring the instrumentation sensitivity

The sensitivity of the TM-1000 SEM-EDS in regards of the elemental analysis was measured in a pre-study. Activated carbon was infused with solutions of dissolved di-sodium molybdate-di-hydrate ($Na_2MoO_4 \bullet 2H_2O$), di-sodium tungstenate-di-hydrate ($Na_2WO_4 \bullet 2H_2O$) sodium bromide (NaBr), manganese(II)chloride-tetra-hydrate ($MnCl_2MoO_4 \bullet 4H_2O$), and di-potassium hydrogen phosphate-tri-hydrate ($K_2HPO_4 \bullet 3H_2O$) salts in deionized water so that a certain weight-% (wt%) of the cations and anions were present. The salts were selected on the basis of having a spread of elements with detection of K_α-

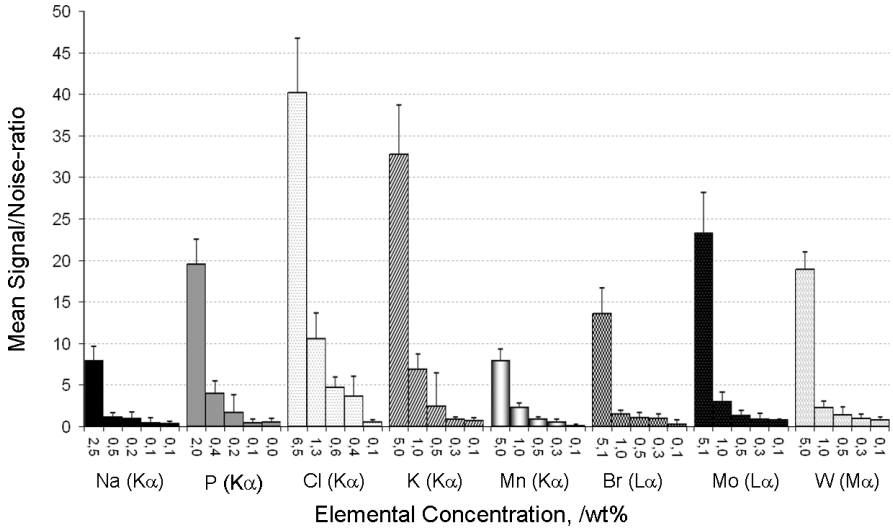

Figure 12. The sensitivity of the EDS-analysis system was tested by infusing activated carbon with solutions of different salts and then dried. The bar-chart shows the signal-to-noise ratios of the EDS analyses made for the carbon with different wt% of the salt species.

, M_α-, and L_α-shell X-ray emissions. The infused carbon was dried and analyzed using EDS area analysis for 3 mins. Figure 12 shows the results of this analysis where the signal-to-noise ratio was extracted from the resulting EDS-spectra. For most elements the sensitivity of detection lies roughly at 0.5 wt%, with Cl and P having slight detectability at just below this limit.

Automated analysis

Automated analysis was performed on the filters in the second study. By setting the instrument to automatically image several regions of the filter and then automatically detecting particles through image contrast enhancement could the number of analyzed particles be raised substantially. Some limits were evident for this method, as the automatic detection had some trouble detecting particles less than 1 μm in size.

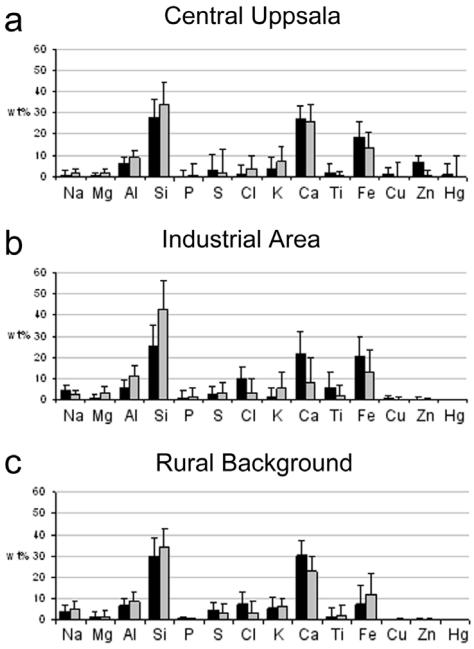

Figure 13. Elemental analysis of the samples for the feasibility study. The background suspended materials Na, Al, Si, Cl, K, and Ca are evident. The main difference is the amount of Fe, being less in the rural background as compared to the central Uppsala and industrial area indicating a possibly technogenic origin. Black = $PM_{2.5}$, grey = PM_{10}.

5.1.3 Elemental composition and prevalence

341 particles in total were analyzed for the first study. The analysis results were expected to show ambient naturally occurring minerals of aluminosilicates, calcium oxides, phophates, potassium and sodium chlorides, and sulphates. Figure 13 outlines the EDS-results for the first study. Indeed, the ambient material is present, but a significant difference being that the amount of Fe (which is considered non-naturally occurring) is higher in the inner city and industrial area compared to the rural background. This relates to the prevalence of technogenic sources (industry, vehicle traffic) in the metropolitan area and which are mostly absent in the rural background. This difference highlights the usefulness of the

method in showing that chemical differences can be observed for individual particles and that an origin of emission can be theorized. More sampling data would be required to draw more detailed conclusions, but the method was shown to be feasible.

The automated analysis provided a total of over 10,000 analyzed particles. This number was reduced by selecting only particles of 10 μm of size and below and additionally eliminating results which had only C and O content (since these are inherently difficult to quantify). This left a total of 2,436 particles. The EDS-analysis reported atomic-% (at%) of elements per particle. To get a clearer total picture, data from the light-scattering equipment (Figure 14) was used to relate the number of particles of a given particle-volume to calculate a coefficient. This coefficient was then used to re-calculate the elemental composition of the particles as based on their number and prevalence at the different collection times and places. The resultant elemental abundance scores can be seen in Figure 15, broken down by element, collection point, and time of collection.

Again the ambient background material, as in the first study, is present. For this particular study the amount of Fe was the most telling. Comparing the

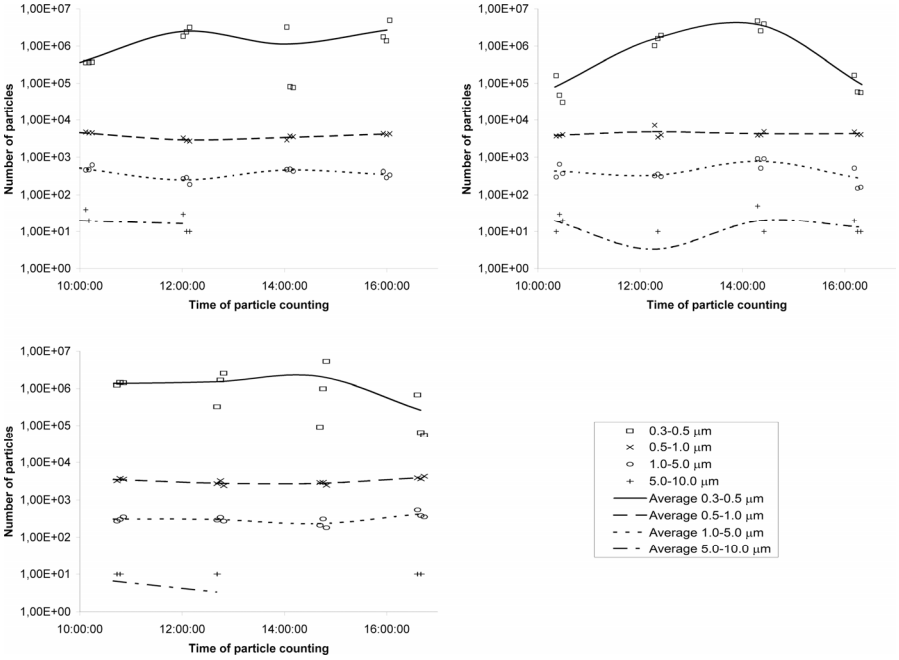

Figure 14. Summary of the particle counter data for the roadside particle study, collection: (top left) roundabout, (top right) roadside, and (bottom left) rural background. Lines represent the averages of the collections (n = 3).

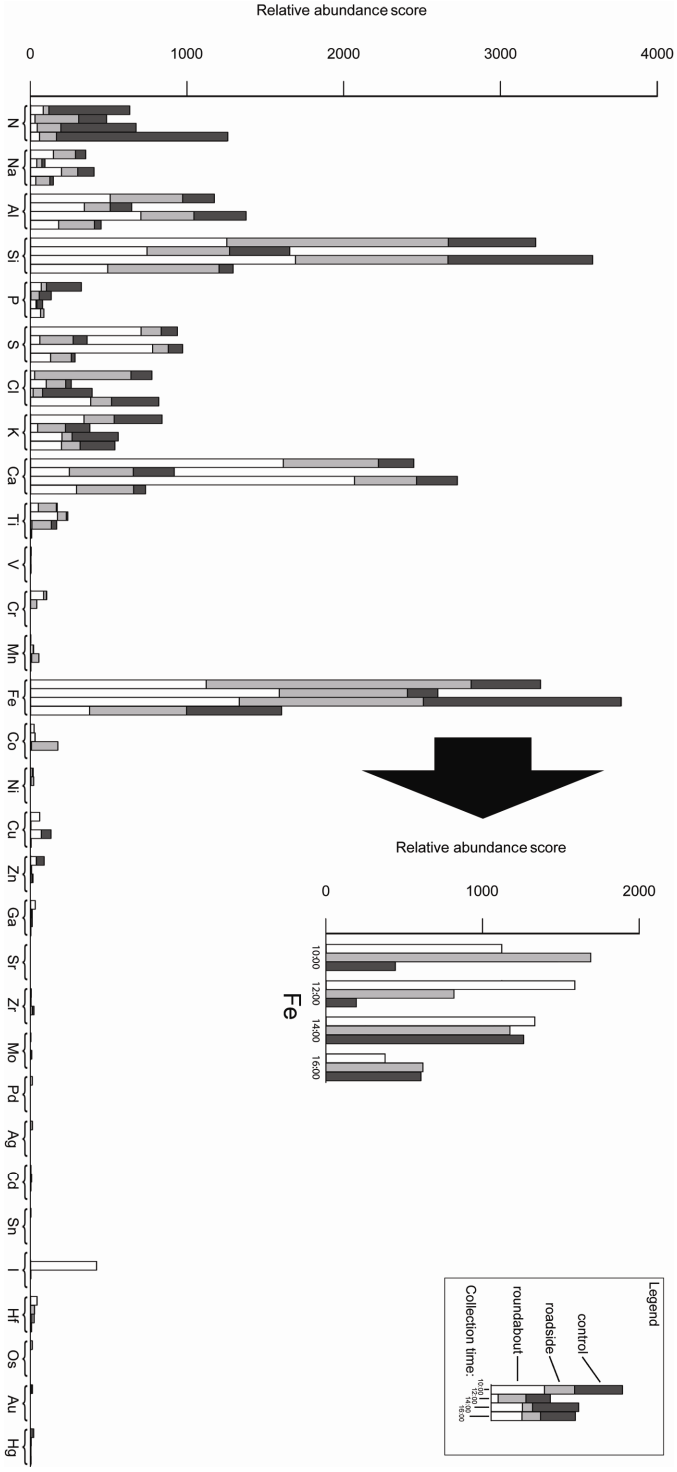

Figure 15. Relative elemental abundance scores for the detected elements for particles from the roadside study. Excerpt shows the breakdown of the bars for Fe as explained by time of collection.

roadside and roundabout amounts of Fe it can be seen that they are considerably elevated at 10 and 12 am if compared with the rural samples. This impact on the other hand is lost at 2 and 4 pm seeing as the amounts are more or less harmonized. This could be an indication that in the morning and at noon the particulates are emitted, but later during the day migrate

away from the road. Towards evening the amounts drop as either the particulates are deposited or they have migrated away from the road and what is left is a harmonized background dust material.

Statistics

The nature of the data for the second study provided some difficulties for PCA-modeling since a high proportion of the data consisted of zero values (no element detected). This meant the data was not normally distributed and parametric statistical methods were not an option. A workaround was made by ranking the data and this in turn made it possible to use the methods. Ranking the data means that the highest value is allotted a number, starting from one, and the highest value after that is allotted the next number and so on. In case of any ties of values the ranks for each would be an average of the allotted ranks.

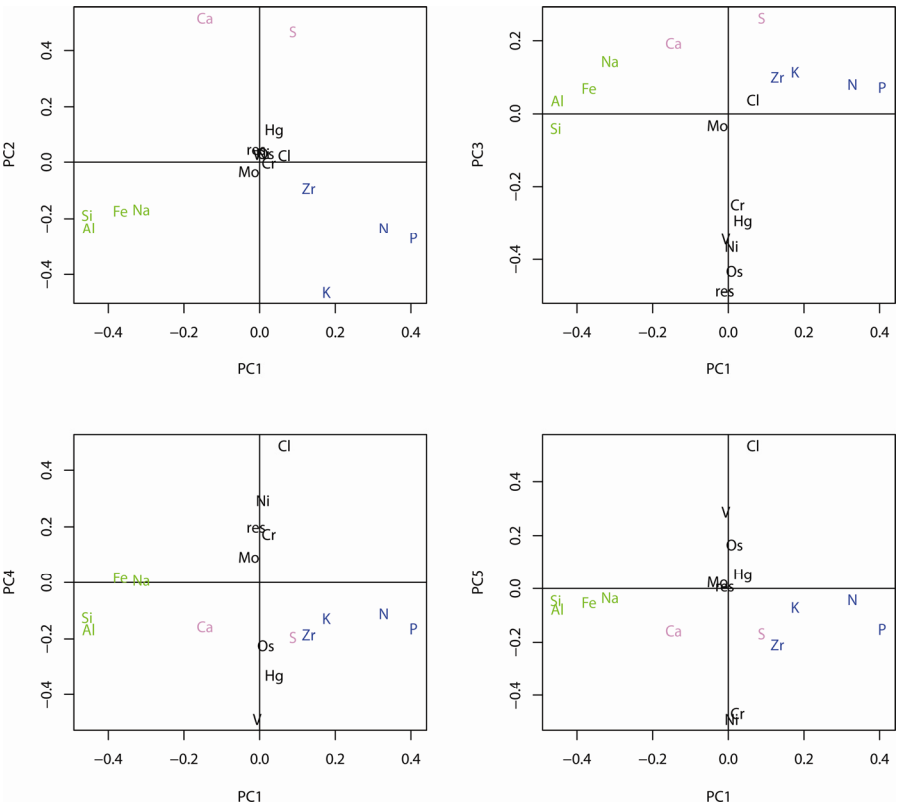

Figure 16. Plots of the loading matrices of PC1 against PCs 2-5. Groupings among variables indicate correlation in the group, idicated by colour code: green = Na, Al, Si, and Fe; blue = N, P, K, and Zr; pink = S and Ca. If opposed by another group on the opposite side of the same axis it indicates negative correlation, e.g. green and blue groups on opposite sides of PC1.

Ranking can cause the occurrence of false positives, that is, if only few values are available the values themselves gain a high ranking which is not necessarily reflected by the elemental content. For this reason certain variables which did not account for a significant quantitative contribution were reduced into one variable called res. In Figure 16 some of the main PC-components of the loading matrices can be seen, usually called a loading plot. The loading plot visualizes the inter-dependency of the loading-values, that is the variables total account for correlation with other variables. Mainly the PC1 plotted against PC2 (Fig. 6, top left) is the plot that explains this variability most closely. From this plot it can be seen that certain element groupings are produced and which have been colour-coded for clarity. PC1 clearly explains the variability within the green group (Na, Al, Si, and Fe) and blue group (N, P, K, and Zr) and additionally adds information that these two groups are

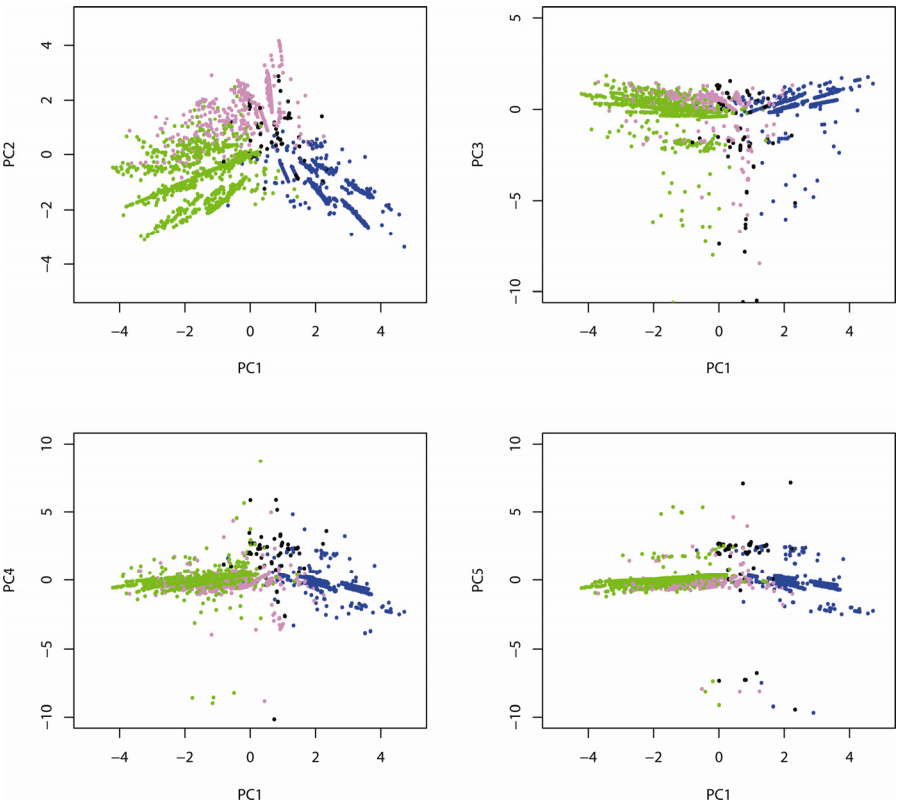

Figure 17. Score plots of PC1 against PCs 2-5. The plots serve as a map of the data points and their respective contribution to the PCs, i.e. how much they 'pull'. Colour-codes are the same as for Figure 16 albeit governed by which element is most present in the particles.

negatively correlated. A third group, pink (S and Ca), is not explained by PC1, but by PC2, separating it from the other groups. What this means is that for a given particle, if the content is rich in elements from the green group then it is probably poor in elements from the blue and pink groups. The groupings offer an explanation in the spreading behaviour of the PM at the roundabout in that Fe is closely related to Si, Al, and Na and is spread together with them.

Figure 17 depicts the scores from each data point and its' contribution to the respective PCs. Usually this type of plot is called a score plot and should be regarded as a map of the samples with respect to the given PCs. In general it follows the same spreading as the loading plot (Figure 16) in that the colour-coded groupings are now represented by each of the particles that were analyzed. The colour-coding here is similar to that from Figure 16 in that the colours given to each particle is governed by which element is most present in the given particle. Each particle can thus be traced to determine how much it correlates with other groups and thus helps to determine the nature of the particle (*e.g.* green dot highly expressed in the direction of PC1 should be Fe-, Al-, Si-, and Na-heavy or any combination of these while the other elements should be absent or low in content).

The data from the PCA-model is still complex and open to some hyperbole. ANOVA was used to determine if any statistical deviations were present. Table 3 lists the specific results from this test, made on the ranked data as for the PCA. As can be seen the time of collection is highly significant in regards to the Fe-content, that is, collection time plays a part in explaining the Fe-content. Looking back at Figure 15 it stands to reason that what the ANOVA is explaining is the disparity between the Fe-content of the 10 and 12 am collections where a difference is observed for roadside and roundabout samples as compared to the rural background. Interestingly no significance is found for the collection placement, but the probability value is still low indicating a general trend might still explain the variance. Probably more data is needed to tell either way.

Table 3. *Tabulated results of the ANOVA for the non-parametric particle Fe-content by particle collection placement and collection time. The analysis proved a 99.9% significance for the time of collection indicating a strong correlation for the amount of Fe and time of collection. Df = degrees of freedom, Sum-sq = sum-of-squares, Mean-sq, mean sum-of-squares, Pr (>F) = probability that the F-value deviates from the tabulated F-value for normal distribution, and DNA = does not apply.*

Variable	Df	Sum-sq	Mean-sq	F-value	Pr (>F)	Significance
Placement	2	841436	420718	1.5075	0.2217	
Time	9	31511522	3501280	12.5459	<2e-16	***
residuals	2424	676483534	279077	DNA	DNA	DNA

Elemental mapping

Determining the particle types and elemental content of a sample of particles can sometimes be tricky and an overview of the contents hard to establish. A test was made to evaluate elemental mapping of a sample. In Figure 18 the results of this can be seen. Elemental information was collected by seven channels: C-K_{α}, O-K_{α}, Na-K_{α}, Al-$K_{\alpha\beta}$, Si-$K_{\alpha\beta}$, Ca-K_{α}, and Au-$M_{\alpha\beta}$ (gold sputter coat, omitted from Fig. 18 since the sample was homogenously covered). Mapping in this way produces an intuitive view of the sample and can help in quickly estimating the types of particles present. If for example a government body were interested in monitoring the chemical components of PM, simplifying the analysis to provide these types of images could remove the need for highly trained professionals needed to interpret complex data and instead ease the monitoring process making it open for a wider audience and user base.

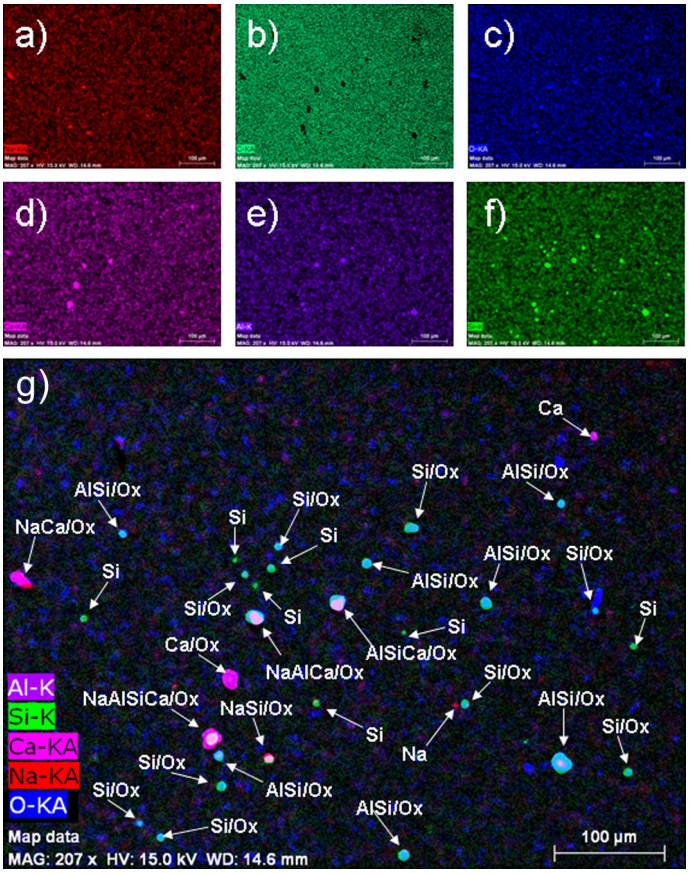

Figure 18. Example of an elemental map on a filter with particles as used in the studies of particle collection and analysis. Slides a-f show the different element channels (Na, C, O, Ca, Al, and Si respectively). Slide g is an interleaved image of the channels with identification marking the occurring particles. Au-channel omitted.

5.2 Synthesized NPs as models for pollution emission and related health effects (Papers III and IV)

5.2.1 Synthesis

The major aim was to synthesize NPs of a hydrophilic nature with a well governed morphology and high crystallinity. To this end, a solvent was needed with a high enough reaction temperature to ensure a highly crystalline product. Although there is a choice of many organic solvents that are available, such as the often used xylene, acetophenone was selected based on a high boiling point (202 °C) and available ketone group. Also acetophenone is a naturally derived aromatic ketone found in fruits and used commercially as a sweetener. As such it had the added potential of being environmentally benign (biodegradable) and if any residues would be present in testing with biological materials, that the solvent residue effects would be negligible.

The synthesis was performed by dissolving an aliquot of the metal acac in acetophenone and then boiled under water-cooled reflux for a determinate amount of hours. By varying the reflux time could the size of the produced NPs be altered. For example, a 4 h synthesis produced magnetite particles of

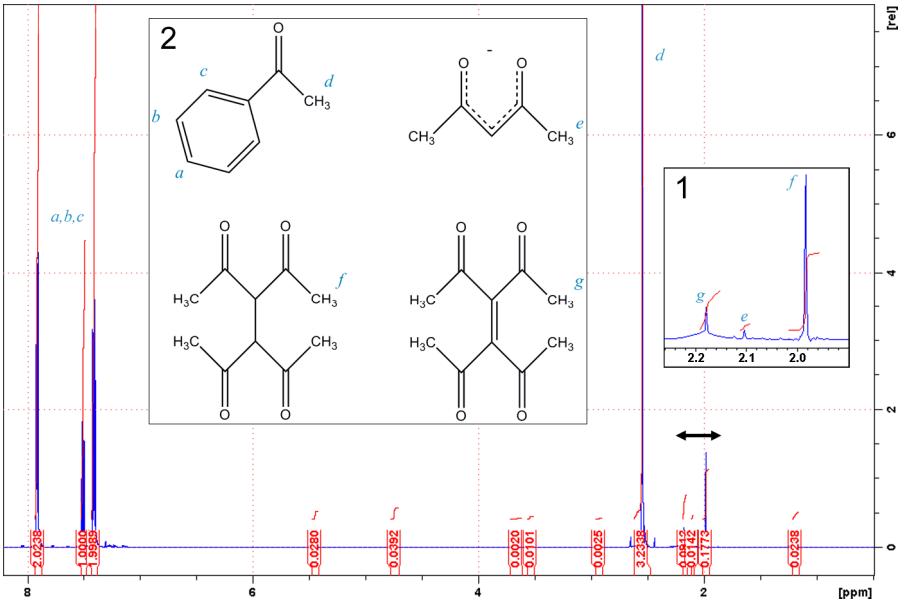

Figure 19. NMR-spectrum of the fresh reaction media of a 4h Pd-NP synthesis. Insert 1 shows a magnification of the area delimited by the arrow-bar. Peaks have been identified by the lettering, as shown in insert 2. Red lines indicate peak integrals. The NMR spectrum for magnetite produced similar results.

roughly 5 nm size, while a 16 h synthesis produced 8 nm particles. Additionally, the longer synthesis seemed to produce a higher crystalline surface phase as the particle transformation to maghemite proceeded more slowly.

At first it was theorized that the reaction taking place in acetophenone was that of the Bradley ether elimination reaction as has been reported for La and Mo. Subsequent analysis of the reaction medium *post synthesis* using NMR, see Figure 19, did not provide proof for the Bradley reaction, instead the reaction taking place was not a reaction between the metal precursor and the solvent, but that of the metal and its chelating ligand acac. From Fig. 19, the distinct species of acac oxidization can be inferred from the ^{1}H-peaks at approx. 2.0, 2.1, and 2.2 ppm (corresponding to the methyl groups in the drawn insert with molecules). *Id est* the metal is being reduced and the acac is oxidized, facilitated by the solvents high boiling point temperature.

5.2.2 Characterization

Extensive characterization was done on the synthesized Pd- and magnetite NPs to detail their characteristics such as size, morphology, crystallinity, behaviour in culture medium in order to better understand the fundamental chemical effects they might pose in live specimens.

The freshly synthesized NPs were dried from any solvents and then ground to a fine powder using a mortar and pestle. The fine powder was then transferred to a 0.7 mm quartz capillary tube and closed off with a torch. A diffraction pattern was then obtained using a Bruker SMART Apex-II

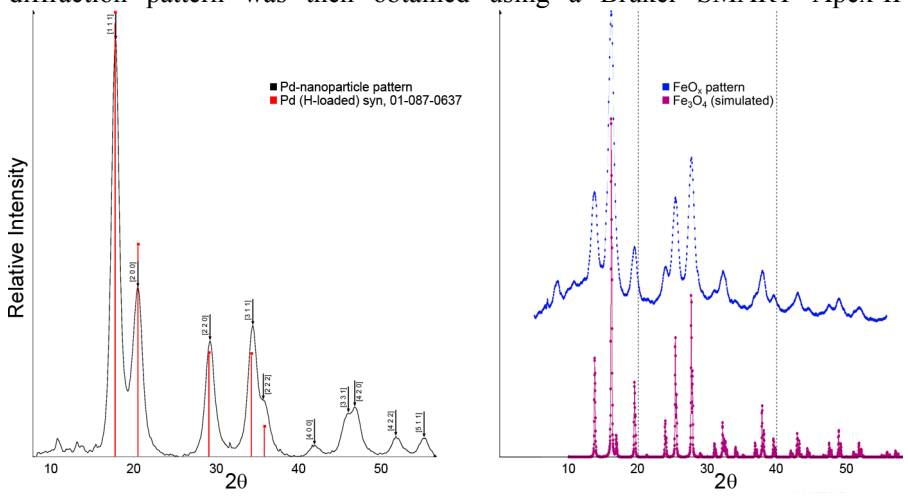

Figure 20. X-ray diffraction patterns for the synthesized Pd-NPs (left), as compared to hydrogen-loaded Pd-metal, and magnetite NPs (right), as compared to a simulated diffraction pattern on magnetite.

diffractometer with a Mo-K_α radiation source (λ = 0.71073 Å). The resulting diffraction patterns were then deconvoluted and compared to select standards. Figure 20 shows the diffraction patterns and as can be seen they conform well to hydrogen-loaded metallic Pd and Fe_3O_4 (magnetite) respectively. For the magnetite NPs, the Debye-Scherrer formula (Eq. 5) was used to calculate the size of the crystallite, *L*:

$$L = \frac{\lambda K}{B_{2\theta} \cos\theta} \qquad \text{(Eq. 5)}$$

where λ is the radiation wavelength, *K* is the peak shape factor (K = 0.9), and $B_{2\theta}$ is the line broadening at full width half maximum (FWHM). Choosing the peak at 2θ at 16.1° L attains the value of 4.1 nm, *i.e.* the crystallite size of the magnetite NPs was 4.1 nm on average.

For more tangible proof of the NPs sizes a Phillips EM-STEM (STEM stands for scanning-transmission electron microscope) or a Phillips Cm-20 SuperTwin were used to image them. A droplet of the NP-suspensions were added to copper grids with a fine carbon film and let to dry. The resulting images can be seen in Figure 21. Since the electron and nuclear density of the magnetite NPs is lower compared to the Pd-NPs it presented some difficulty in imaging them (Fig. 21a). Nonetheless the primary size of the particles can be estimated at being approximately 5 nm. While this size may deviate some from that calculated from Eq. 5, it has to be noted that the Debye-Scherrer method provides the size of the primary crystallite. Thus it can be assumed that the core of the magnetite NPs is roughly 4.1 nm of highly crystalline magnetite covered by a 0.5 nm thick layer of amorphous or aphasic magnetite. Figure 21b shows the primary size of the Pd-NPs and calculating the sizes (Fig. 21d) provides a uniform size-distribution of 10.4 ± 2.7 (one standard deviation). Figure 21c shows the synthesized Pd/Al_2O_3-nanocomposite as a dried-up cluster.

Assessing the behaviour of NPs in aqueous solutions is important if the aim is to use them for assessing their cytotoxicological effects in live cells. Since NPs have an excessive surface-to-bulk ratio the surface characteristics govern the NPs properties when in contact with a liquid, especially that of surface charge. Depending on the NPs properties, a surface charge may develop in aqueous solutions if other prerequisites are met, such as the ionic strength, pH, surface binding moieties *etc.* leading to a possible agglomeration of NPs into larger agglomerated particles. For the synthesized Pd- and magnetite NPs their behaviour in a variety of culture media suspensions (the same as used for culturing the cells used in the cytotoxicity studies) was investigated by means of NTA and DLS measurements (NanoSight LM10 HSB and Malvern Z-Sizer

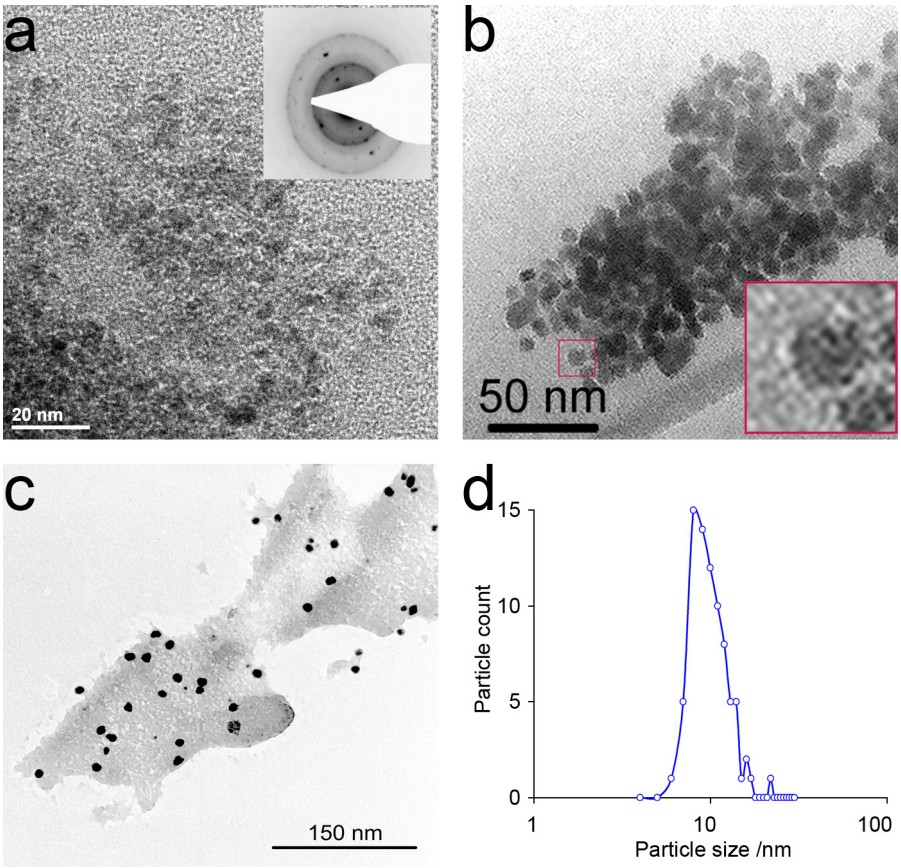

Figure 21. TEM images of magnetite- and Pd-NPs. a) Magnetite NPs from a 16 h synthesis. Insert shows a SAD diffraction pattern for the particles proving their crystallinity. b) Pd-NPs from a 4 h synthesis. Insert shows a magnification of one particle illustrating the spherical morphology. c) Pd/Al-nanocomposite. Pd-NPs (black spots) on a dry deposit of Al-NPs. d) Size-distribution of synthesized Pd-NPs.

respectively) and the results can be seen in Figure 22. Taking Pd-NPs as an example, two peaks (MilliQ-water and PBEC in Fig. 22 [top and center]) are roughly in the same size region around 100 nm, *i.e.* the 10.4 nm particles agglomerate in solution to form larger agglomerates of approximately 100 nm size. An interesting deviation is seen for the DLS measurement of Pd-NPs in A549 culture medium where they do not seem to form agglomerates, yet the NTA measurement shows that they do. A hypothesis is that what is seen in the NTA measurement are protein micelles and which do not show up in the DLS measurement since it uses a fixed refractive index (for Pd) and does not detect protein micelles. These same proteins, or possibly others, may be acting as

stabilizers of the NPs in the solution and thus hindering agglomeration, providing individual particles. For the NTA measurement, these cannot be seen as they are too small to adequately reflect light and be detected. DLS also provided z-potential measurements for the Pd-NPs, which were close to zero for water, -15.3 for PBEC and -12.8 for A549 (mV). For the magnetite NPs (Fig. 22, bottom) a large peak can be seen between 30-250 nm, measured for RPMI cell culture medium with 10% added fetal calf serum (FCS).

5.3 Cytotoxicological effects

Gaining information on particle exposure and related health effects are an important step in understanding how they interact with the human body and aiding risk assessment in for example hazardous occupational situations or general exposure. To this end, the synthesized and characterized Pd- and magnetite NPs were used in *in vitro* tests where live cells were subjected to these NPs.

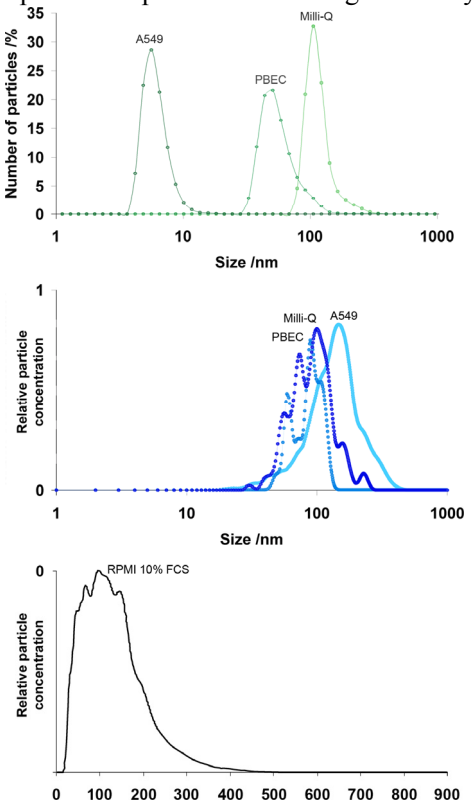

Figure 22. Size-distribution profiles for NPs in different solutions. (top) DLS measurement on Pd-NPs in MilliQ-filtered de-ionized water, PBEC-, and A549-culture medium. (center) NTA measurements on Pd-NPs in the same solutions as (top). (bottom) NTA measurement on magnetite NPs made in RPMI 10% FCS culture medium.

PBEC and A549 cells were used as an exposure model for the human airway as PBEC cells served as a model for bronchial epithelial cells (upper bronchial region) and A549 cells used as a model for alveolar epithelial cells (lower gas-exchange region). The toxic effects originating specifically from Pd-NPs were investigated by means of trypan blue (vital dye) exclusion in cells exposed to a 25 µg/ml NP concentration (Figure 23a). After a 24 hour exposure a clear disparity exists as PBEC cells were almost totally non-viable while A549 were slightly affected but almost wholly viable. The dose-dependent toxicity was investigated by

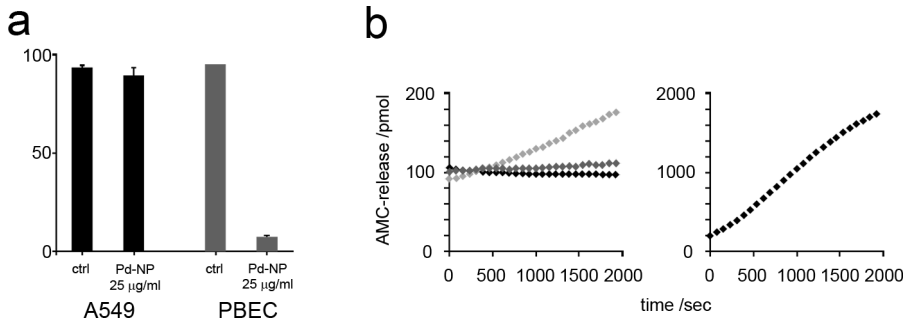

Figure 23. a) Cell viability for A549 (left) and PBEC cells (right) exposed for 24 hours to 25 μg/ml of Pd-NP as compared to an untreated control, measured by trypan blue exclusion. b) Measure of the AMC-release as an indicator of caspase-3-like enzyme activity from the cell lysate of PBEC cells. (b, left) black = control, grey = 10 μg/ml Pd-NP, and light grey = 25 μg/ml Pd-NP. (b, right) Staurosporine positive control.

measuring AMC-release in the cell cytoplasm. DEVD-AMC (Asp-Glu-Val-Asp-7-amino-4-methylcoumarin) is a fluorogenic substance and when cleaved by caspase 3 is indicative of caspase-3-like enzyme activity. Activity of caspase 3 and related orthologs in cells are central when the cell undergoes apoptosis and serve as a marker for when cells are stressed and undergo programmed cell death. Figure 23b shows a real-time measurement of cells exposed to Pd-NPs and the subsequent release of AMC over time. It is clear that, if compared to the non-treated control, a correlation with amount of NP exposure and AMC release is evident. Furthermore a positive control was made by subjecting cells to a known protein kinase inhibitor (which induces apoptosis) staurosporine (STS) for reference.

Figure 24 shows TEM-slides of A549 and PBEC cells subjected to 10 μg/ml of Pd-NPs for 2 hours. The A549 alveolar cells (Figs. 24a and b) did not take up any cells and maintained them outside of the cell membrane. PBEC cells however showed Pd-NPs inside the cells (Figs. 24c and d). The NPs were mostly collected into vacuoles. It is unknown whether these vacuoles are a direct result of the cells concentrating the NPs in the vacuoles separating them from the cytoplasm or that the vacuoles were generated as a result of the Pd chemistry. Even though cytoxicity was observed in both cell types, it was more pronounced in PBEC cells. Figure 24e shows PBEC cells that have become necrotic as a result of the Pd-NP exposure. Cells exposed to the Pd/Al_2O_3-nanocomposite showed a dose-dependent toxicity similar to cells exposed only to Al-NPs (data not shown) and is in agreement of other similar observations for Al-toxicity [Braydich-Stolle 2010]. Al is known to leach Al^{3+} ions causing a toxic response and is more potent toxicity-wise than the Pd-NPs.

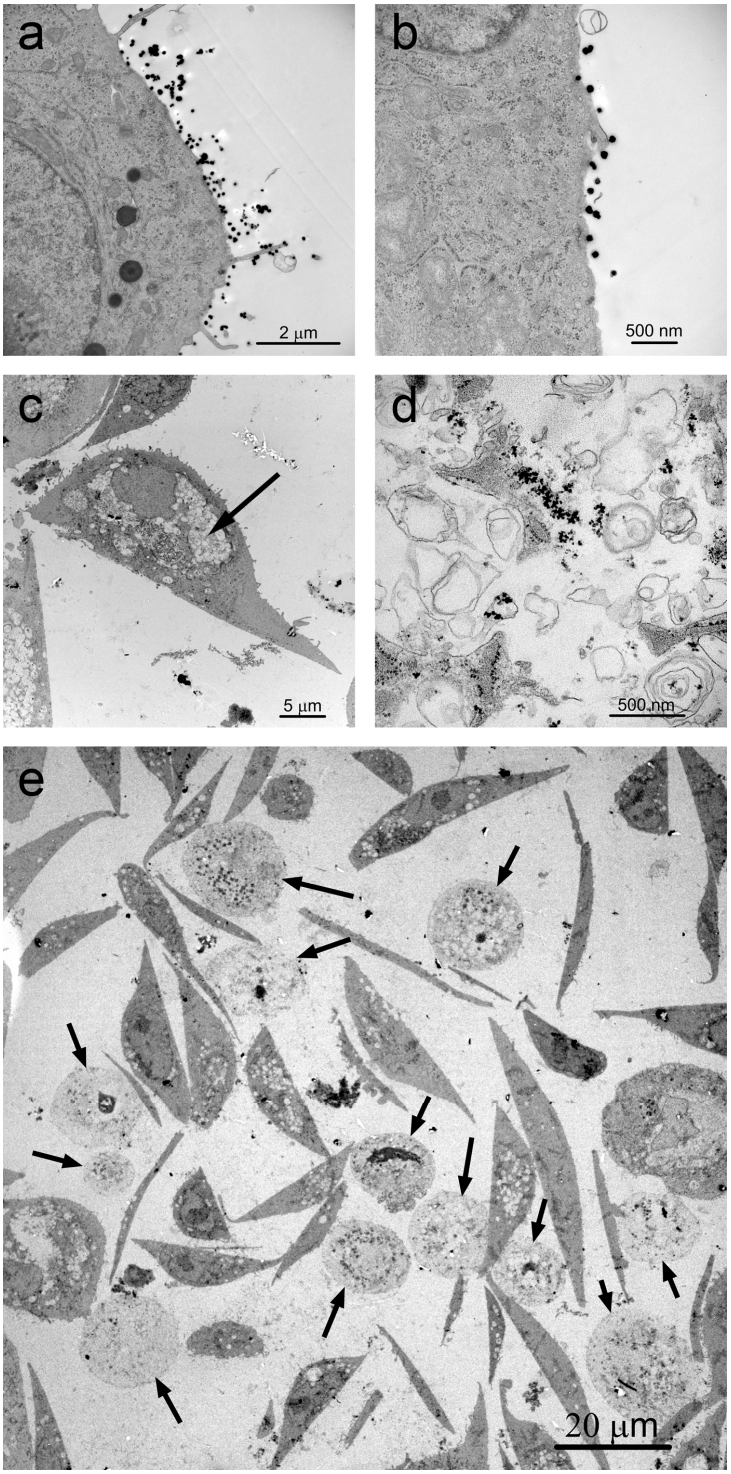

Figure 24. TEM images of A549 and PBEC cells subjected to 10 µg/ml of Pd-NPs for 2 h. a) and b) A549 cell (grey) with Pd-NPs on the surface of the cell (black spots). c) PBEC cell with arrow pointing at the magnification in d). d) Evidence of internalization of Pd-NPs in PBEC. e) Necrotic PBEC cells (shown by arrows) as a consequence of exposure to Pd-NPs.

The difference in toxicity for A549 and PBEC cells exposed to the same materials in the same concentrations is interesting. Three plausible options exist to explain this phenomenon: I) alveolar cells are more resistant to Pd-NP toxicity due to being an immortalized cancer cell line having developed a resistance to apoptosis induction; II) Protein opsonization played a part in uptake for PBEC as the culture medium included a 10% addition of serum (A549 culture medium did not contain serum, but some growth hormones); III) the time for the uptake action of the cells differ in time and two hours of cultivation was not enough time to show the uptake in A549. Ironing out the cause for the uptake discrepancy is a complex issue and probably no one explanation is true, rather a mixture of options is more plausible. Regardless, more data on Pd-NP uptake would be needed to draw deeper conclusions.

A different approach was taken to show the specific toxicity of magnetite NPs in that the cell models chosen were: I) human Epstein-Barr-virus transformed 721.221 B-cell line as a suspension model for lymphocytes; II) adherent human embryonic kidney 293T (HEK293T) cell line as a model for kidney cells; and III) A549 cells were again used as a model for pulmonary cells. The selection of cell types was done to get a totalistic view of the NPs as they impacted the pulmonary system (A549-cells), where they are taken up into the body and feasibly come into contact with immune defence cells (221 B-cells) and furthermore upon clearance from the body come into contact with renal kidney cells (293T-cells).

It was theorized that if particles that were subject to opsonization of proteins somehow were recognized differently by the host cell that perhaps adenosine-tri-phosphate (ATP) modified magnetite NPs would do the same, that the ATP helped the magnetite NPs enter the cells and once there be coordinated toward the mitochondria of the cells. A549 cells were subjected for 24 hours to varying concentrations of (ATP) surface modified and unmodified magnetite NPs. The release of interleukin 8 (IL-8) can be used as an indicator for a pro-inflammatory response by the host cell. Figure 25a shows the levels of release depending on the concentration

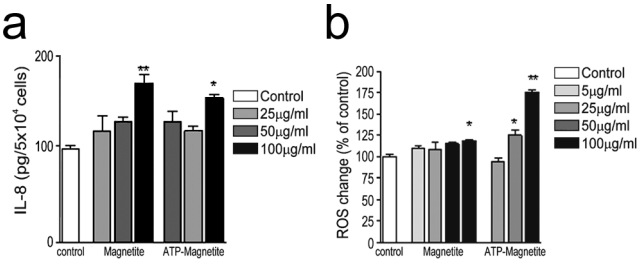

Figure 25. Bioassays showing A549 cell response to magnetite NPs. a) IL-8 release measured by enzyme-linked immunosorbent assay (ELISA). b) Change in ROS formation as a result of superoxide reduction.

of magnetite NPs. Slightly heightened levels of IL-8 were present for the A549 cells subjected to magnetite NPs compared to the control indicating an inflammatory response in a general dose-dependent manner. Additionally the change in ROS formation was followed by the reduction caused by superoxide as seen in Figure 25b. ROS change was slightly elevated but interestingly the ATP-modified NPs caused a significant amount of ROS formation. This could be indicative that they indeed were directed in the cell to a place where they could exert their toxicity, *e.g.* the mitochondria. This is supported by Raman spectroscopy measurements of A549 cells subjected to magnetite NPs. Raman spectra were collected from regions inside A549 cells subjected to unmodified magnetite NPs producing the spectra seen in Figure 26a. Magnetite has a characteristic Raman band in the 700 cm^{-1} region which is seen in both spectra in Figure 26. In comparison A549 cells were subjected to ATP-modified magnetite NPs resulting in the spectra in Fig. 26b. The spectra shows fluorescence from that of the ATP indicating that indeed the NPs are internalized in the cells and that the toxic effects are occurring within the cell.

The cell proliferation of 221 B-cells and 293T-cells for varying doses of magnetite NPs were monitored over time using confocal light microscopy. Figure 27 shows the confocal images of vital dye coloured cells every 24 hours with the corresponding dose of NPs making it clear that doses 1.0-20 μg/ml have a negative impact on the cells. This is further reinforced by the cell counts (line charts at bottom of Fig. 27). Doses of 10 and 20 μg/ml have a clear impact on cell mortality virtually killing them off in the first 24 hours. In contrast to the A549 cells, the 221 and 293T cells seem to be more sensitive to magnetite NP exposure. This could be explained by the fact that A549 cells have a natural resistance to foreign bodies due to their placement in the lungs

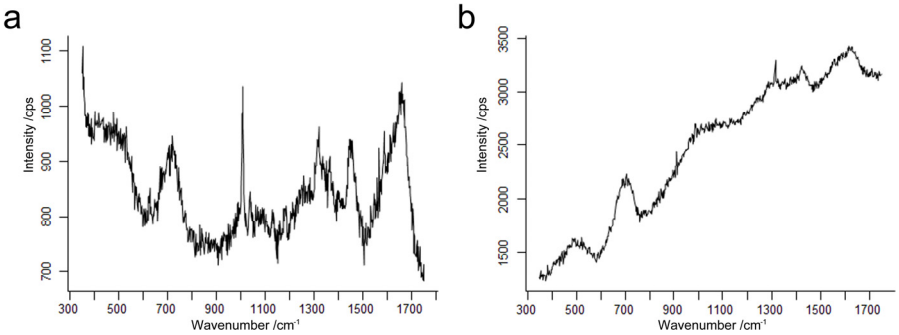

Figure 26. Raman spectroscopy measurements of A549 cells subjected to magnetite NPs. a) Raman spectra from inside of A549 subjected to unmodified magnetite NPs and b) spectra from cells with ATP-modified magneite NPs.

and acting as a safeguard to ward of hazardous materials. The immune cells on the other hand have very specific roles in the body and are not accustomed to handling foreign bodies.

When magnetite comes into contact with an oxidative environment, like *e.g.* an aqueous solution, it undergoes oxidation and turns into maghemite. This reaction has a first order rate of reaction of 0.052 h^{-1}. Since cell testing is done using aqueous cell media it is plausible to assume that the magnetite oxidizes into maghemite and possibly its' toxic potential alters over time. This was investigated by a cell proliferation study on A549 using the most common forms of iron oxide materials. Figure 28 shows a line chart of the results of the study: hematite seems to be the most toxic iron oxide form followed by

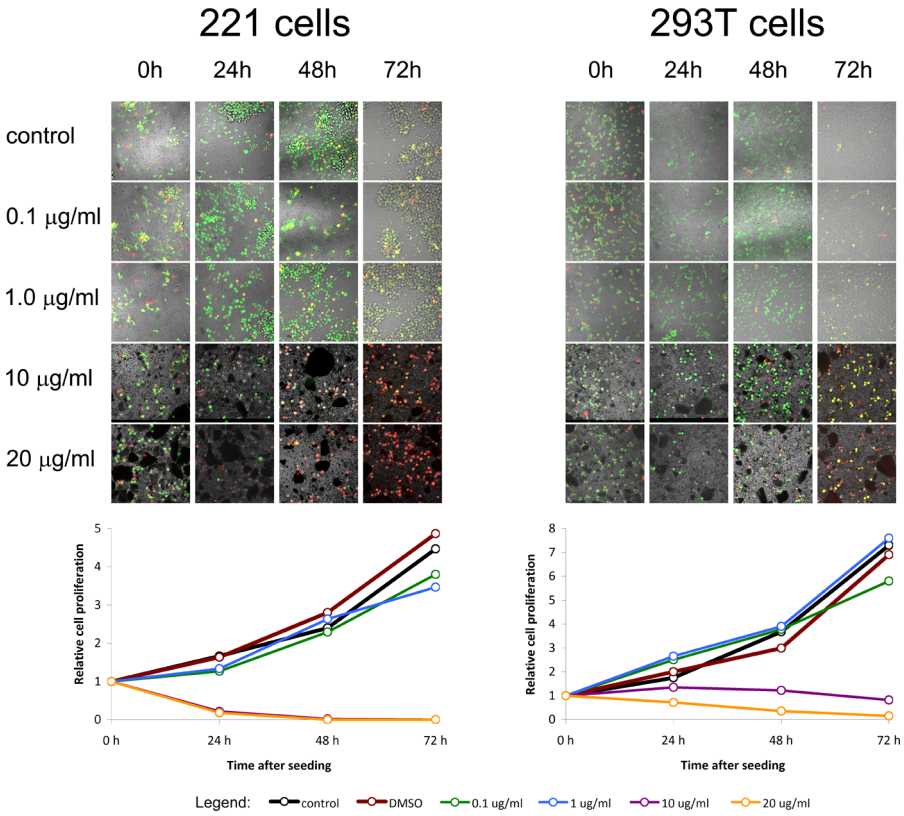

Figure 27. Cell proliferation study of 221 cells (left) and 293T cells (right) cultured with different concentrations of magnetite NPs as imaged by confocal light microscopy. Top scale is the time of imaging after sowing the cells and side scale is the concentration of NPs in the cell medium. Cells which are green in colour are still viable while the red coloured cells indicate necrotic or dead cells. Cell counts are summarized in the below graphs with the addition of a culture with DMSO reaction medium, essentially a control of the effects of the DMSO reaction medium of the particles.

maghemite, magnetite, and lastly by goethite. The toxic impact from magnetite is comparable with maghemite and leads to the conclusion that no specific considerations are needed to account for the different iron oxide phase transmutations.

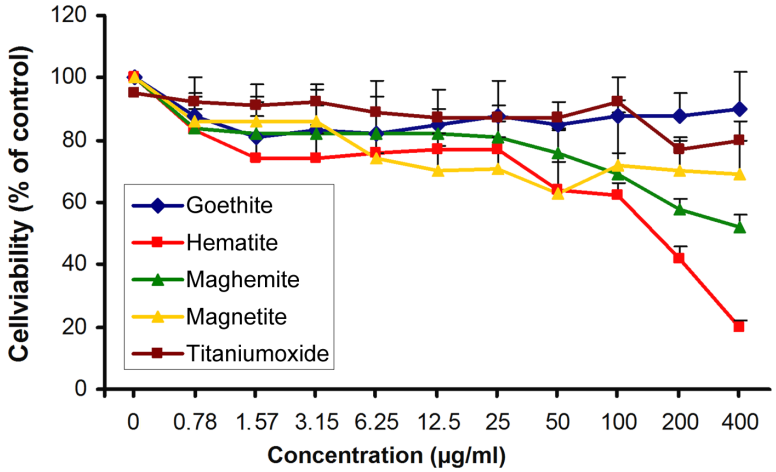

Figure 28. Cell viability of A549 cells when subjected to NPs of the most common iron oxide phases, by concentration. The titaniumoxide used was the standard P25 TiO_2.

6 Conclusions

The feasibility of collection and express analysis of airborne particulate matter was shown by a proof-of-concept study using custom particle capturing and miniaturized SEM-EDS equipment. A method was developed by which individual particles captured on-site onto nucleopore filters were analyzed for their chemical content, and depending on place of collection, differences in the chemical content were observed.

Further development of the express analysis technique was done by employing automated EDS-analysis. Particulates were captured from distinct points from a model system consisting of a heavily utilized roundabout. The subsequent high-volume analysis proved marked differences in amounts of particles and chemical content dependent on time and place of collection.

Model fractions of technogenic magnetite and metallic palladium nanoparticles were synthesized by wet chemistry and extensively characterized by TEM, XPD, NTA, and DLS. These were then used in model *in vitro* cell culture systems simulating the human airway epithelial-, immunological-, and renal cells to test for the toxic impact from the particulates. It was found that both magnetite and Pd particles exhibited toxicity at relatively high amounts, but inflammatory markers showed an adverse impact also for lower concentrations. Additionally the airway cells seem to possess a measure of natural resistance to particulates, whereas immunological and renal cells were negatively affected at rather low concentrations.

Future outlook

The interest in particulate pollutant effects on humans is increasing due to the potential long-term health risks associated with exposure. A large part of the specific mechanisms by which particulates exhibit toxicity is poorly understood and warrants further investigation. To this end new technology and techniques are continuously being developed such as the miniaturization of

measuring and analysis equipment to give more conclusive results. Also, *in vitro* studies are being developed where cells are cultivated on air-lift beds to simulate actual tissue studying the effects at the cell-particle air-liquid interface. This technique holds promise as thus far *in vitro* studies are limited to model systems that are not necessarily in accord with what is really happening. By using these types of systems a more complete picture can be made of what the real effects of particulate exposure mean. 8By increasing knowledge on the negative effects can measures be taken to limit exposure. Some particulates have exotic properties which may be harnessed for good in medical applications such as targeted drug delivery. The electronics industry is producing new products with nanoengineered particles at an alarming rate. As the development and use of nanomaterials increases, new unforeseen effects may be observed if we are exposed to them, so maintaining a constant vigil on particulates is surely the way of the future.

References

Acres, G. J. K.; Harrison, B. (2004). The Development of Catalysts for Emission Control from Motor Vehicles: Early Research at Johnson Matthey. *Top Catal*, vol. 28, pp. 3-11.

Aitken, R. J.; Chaudhry, M. Q. ; Boxall, A. B. A. ; Hull, M. (2006). Manufacture and Use of Nanomaterials: Current Status in the UK and Global Trends. *Occup Med*, vol. 56, pp. 300-306.

Andersson, P. O.; Lejon, C.; Ekstrand-Hammarström, B.; Akfur, C.; Ahlinder, L.; Bucht, A.; Österlund, L. (2011). Polymorph- and Size-Dependent uptake and Toxicity of TiO_2 Nanoparticles in Living Lung Epithelial Cells. *Small*, vol. 7, pp. 514-523.

Apopa, P. L.; Qian, Y.; Shao, R.; Lan Guo, N.; Schwegler-Berry, D.; Pacurari, M.; Porter, D.; Shi, X.; Vallyathan, V.; Castranova, V.; Flynn, D. C. (2009). Iron Oxide Nanoparticles Induce Human Microvascular Endothelial Cell Permeability Through Reactive Oxygen Species production and Microtubule Remodeling. *Particle and Fibre Toxicology*, vol. 6, pp. 1-14.

Bangert, H.; Eisenmenger-Sittner, C.; Bergauer, A. (1996). Deposition and Structural Properties of Two-component Metal coatings for Tribological Applications. *Surface and Coatings Technology*, vol. 80, pp. 162-170.

Barnard, C.; Gilbert, F.; McGregor, P. (2001). Asking Questions in Biology: Key Skills for practical Assessments and Project Work, 2nd ed. *Pearson Education Ltd., London, UK*. ISBN: 0-130-90370-1.

Bond, T. C. (2007). Can Warming Particles Enter Global Climate Discussion? *Environ Res Lett*, vol. 2, pp. 1-9.

Braydich-Stolle, L. K.; Speshock, J. L.; Castle, A.; Smith, M.; Murdock, R. C.; Hussain, S. M. (2010). Nanosized Aluminum Altered Immune Function. *ACS Nano*, vol. 4, pp. 3661-3670.

Buzea, C.; Pacheco, I. I.; Robbie, K. (2007). Nanomaterials and nanoparticles: Sources and Toxicity. *Bio Inter Phases*, vol. 2, pp. MR17-MR71.

CARB (1990), Method 501: Determination of Size Distribution of Particulate Matter from Stationary Sources. *State of California Air Resource Board.*

Card, J. W.; Zeldin, D. C.; Bonner, J. C.; Nestmann, E. R. (2008). Pulmonary Applications and Toxicity of Engineered Nanoparticles. *Am J Physiol Lung Cell Mol Physiol*, vol. 295, pp. L400-L411.

Cedervall, T.; Lynch, I.; Lindman, S.; Berggård, T.; Thulin, E.; Nilsson, H.; Dawson, K. A.; Linse, S. (2007). Understanding the Nanoparticle-Protein Corona Using Methods to Quantify

Exchange Rates and Affinities of Proteins for Nanoparticles. *P Natl A Sci*, vol. 104, pp. 2050-2055.

Colombo, C.; Monhemius, A. J.; Plant, J. A. (2008). Platinum, Palladium and Rhodium Release from Vehicle Exhaust Catalysts and Road Dust Exposed to Simulated Lung Fluids. *Ecotox Environ Safe*, vol. 71, pp. 722-730.

Cornell, R. M.; Schwetmann, U. (2003). The Iron Oxides: Structure, Reactions, Occurences and Uses. *WILEY-VCH Verlag GmbH & Co., KGaA, Weinheim*. ISBN: 3-527-30274-3.

Directive 2008/50/EC (2008). Directive 2008/50/EC of the European Parliament and of the Council of May 2008 on Ambient Air Quality and Cleaner Air for Europe. *Official Journal of the European Union*, L152, pp.1-44.

Dockery, D. W.; Pope III, C. A.; Xu, X.; Spengler, J. D.; Ware, J. H.; Fay, M. E.; Ferris Jr., B. G.; Speizer, F. E. (1993). An Association Between Pollution and Mortality in six U.S. Cities. *New Engl J Med*, vol. 329, pp. 1753-1759.

Donaldson, K.; Borm, P. J. A.; Castranova, V.; Gulumian, M. (2009). The Limits of Testing Particle-Mediated Oxidative Stress In Vitro in Predicting Diverse Pathologies; Relevance for Testing of Nanoparticles. *Particle and Fibre Toxicology*, vol. 6, doi: 10.1186/1743-8977-6-13.

Donaldson, K.; Murphy, F. A.; Duffin, R.; Poland, C. A. (2010). Asbestos, Carbon Nanotubes and the Pleural Mesothelium: A Review and the Hypothesis Regarding the Role of Long Fibre Retention in the Parietal Pleura, Inflammation and Mesothelioma. *Particle and Fibre Toxicology*, vol. 7, doi: 10.1186/1743-8977-7-5.

Dziendzikowska, K.; Gromadzka-Ostrowska, J.; Lankoff, A.; Oczkowski, M.; Krawczyńska, A.; Chwastowska, J.; Sadowska-Bratek, M.; Chajduk, E.; Wojewódzka, M.; Dušinska, M.; Kruszewski, M. (2012). Time-Dependent Biodistribution and Excretion of Silver Nanoparticles in Male Wistar Rats. *J Appl Toxicol*, vol. 32, pp. 920-928.

Esbensen, K. H. (2002). Multivariate Data Analysis in Practice. *CAMO Process AS, Oslo, Norway*. ISBN: 82-993330-3-2.

Fadeel, B.; Pietroiusti, A.; Shvedova, A. A. (2012). Adverse Effects of Engineered Nanomaterials: Exposure, Toxicology, and Impact on Human Health. *Elsevier Academic Press, London, UK*. ISBN: 978-0-12-386940-1.

Feng, J.; Huili, L.; Bhakoo, K. K.; Lu, L.; Chen, Z. (2011). A Metabonomic Analysis of Organ Specific Response to USPIO Administration. *Biomaterials*, vol. 32, pp. 6558-6569.

Fenger, J. (1999). Urban Air Quality. *Atmos Environ*, vol. 33, pp. 4877-4900.

Filipe, V.; Hawe, A.; Juskoot, W. (2010). Critical Evaluation of Nanoparticle Tracking Analysis (NTA) by NanoSight for the Measruement of Nanoparticles and protein Aggregates. *Pharm Res*, vol. 27, pp. 796-810.

Foltescu, V. L. ; Selin Lindgren, E. ; Isakson, J. ; Öblad, M.; Pacyna, J. M.; Benson, S. (1996). Gas-To-Particle Conversion of Sulphur and Nitrogen Compounds as Studies at Marine Stations in Northern Europe. *Atmos Environ*, vol. 30, pp. 3129-3140.

Fox, D. L. (1997). Air Pollution. *Anal Chem*, vol. 69, pp. 1R-13R.

Furusjö, E. ; Sternbeck, J. ; Palm Cousins, A. (2007). PM_{10} Source Characterization at Urban and Highway Roadside Locations. *Sci Total Environ*, vol. 387, pp. 206-219.

Geiser, M.; Kreyling, W. (2010). Deposition and Biokinetics of inhaled Nanoparticles. *Particle and Fibre Toxicology*, vol. 7, pp. 1-17.

Genzleben, C.; Pelsy, F.; Foss Hansen, S.; Corden, C.; Grebot, B.; Sobey, M. (2011). Review of Environmental Legislation for the Regulatory Control of Nanomaterials, *DG Environment, European Commision*, Contract No. 070307/2010/580540/SER/D.

Giordano, S.; Adamo, P.; Spagnuolo, V. ; Vaglieco, B. M. (2010). Instrumental and Bio-Monitoring of Heavy Metal and Nanoparticle Emissions from Diesel Engine Exhaist in Controlled Environment. *J Environ Sci*, vol. 22, pp. 1357-1363.

Glaister, B. J.; Mudd, G. M. (2010). The Environmental Costs of Platinum-PGM Mining and Sustainability: Is the Glass Half-Full or Half-Empty? *Miner Eng*, vol. 23, pp. 438-450.

Godoi, R. H. M.; Braga, D. M.; Makarovska, Y.; Alfoldy, B.; Carvalho Filho, M. A. S.; Van Grieken, R.; Godoi, A. F. L. (2008). Inhalable Particulate Matter from Lime Industries: Chemical Composition and Deposition in Human Respiratory Tract. *Atmos Environ*, vol. 42, pp. 7027-7033.

Goldstein, J. I.; Newbury, D. E.; Echlin, P.; Joy, D. C.; Lyman, C. E.; Lifshin, E.; Sawyer, L.; Michael, J. R. (2007). Scanning Electron Microscopy and X-Ray Microanalysis. *Springer Science + Business Media LLC, New York, USA*. ISBN: 978-0-306-47292-3.

Golobič, M.; Jemec, A.; Drobne, D.; Romih, T.; Kasemets, K.; Kahru, A. (2012). Upon Exposure to Cu nanoparticles, Accumulation of Copper in the Isopod *Porcellio scaber* is due to Dissolved Cu Ions Inside the Digestive Tract. *Environ Sci Technol*, vol. 46, pp. 12112-12119.

Goncalves, A.; Domínguez, J. R.; Alvarado, J. (2008). Determination of Pd, Pt and Rh in vehicles escape fumes by GF-AAS and ICP-OES. *Talanta*, vol. 75, pp. 523-527.

Gottschalk, F.; Sonderer, T.; Scholz, R. W.; Nowack, B. (2009). Modeled Environmental concentrations of Engineered Nanomaterials (TiO_2, ZnO, Ag, CNT, Fullerenes) for Different Regions. *Environ Sci Technol*, vol. 43, pp. 9216-9222.

Gustaffson, M.; Blomqvist, G.; Gudmundsson, A.; Jonsson, P.; Swietlicki, E. (2011). Dust Formation Propensity of Road Pavements. VTI Swedish National Road and Transport Research Institute, *Report 711, Linköping, Sweden*.

Hikosaka, K.; Kim, J.; Kajita, M.; Kanayama, A.; Miyamoto, Y. (2008). Platinum Nanoparticles have an Activity Similar to Mitochondrial NADH: Ubiquinone Oxidoreductase. *Colloid Surface B*, vol. 66, pp. 195-200.

Häfell, U. O.; Riffle, J. S.; Harris-Shekhawat, L.; Carmichael-Baranauskas, A.; Mark, F.; Dalley, J. P.; Bardenstein, D. (2009). *Mol Pharm*, vol. 6, pp. 1417-1428.

Ilyinskaya, E.; Martin, R. S.; Oppenheimer, C. (2012). Aerosol Formation in Basaltic Lava Fountaining: Eyjafjallajökull Volcano, Iceland. *J Geophys Res*, vol. 117, doi:10.1029/2011JD016811.

Isakson, J. ; Öblad, M. ; Selin Lindgren, E.; Djupström Fridell, M.; Pacyna, J. M.; Mäkinen, M. (1997). Perturbation of Background Aerosol at Rural Sites in the Nordic Countries. *Atmos Environ*, vol. 31, pp. 3077-3086.

Karlsson, H. L.; Gustafsson, J.; Cronholm, P.; Möller, L. (2009). Size-Dependent Toxicity of Metal Oxide Particles – A Comparison Between Nano- and Micrometer Size. *Toxicol Lett*, vol. 188, pp. 112-118.

Kašpar, J.; Fornasiero, P.; Hickey, N. (2003). Automotive Catalytic Converters: Current Status and some Perspectives. *Catal Today*, vol. 77, pp. 419-449.

Katsnelson, B.; Privalova, L. I.; Kuzmin, S. V.; Degtyareva, T. D.; Sutunkova, M. P.; Yeremenko, O. S.; Miinigalieva, I. A.; Kireyeva, E. P.; Khodos, M. Y.; Kozitsina, A. N.;

Malakhova, N. A.; Glazyrina, J. A.; Shur, V. Y.; Shishkin, E. I.; Nikolaeva, E. V. (2010). Some Peculiarities of Pulmonary Clearance Mechanisms in Rats after Intratracheal Instillation of Magnetite (Fe_3O_4) Suspensions with Different Particle Sizes in the Nanometer and Micrometer Ranges: Are We Defenseless against Nanoparticles? *Int J Occup Environ Health*, vol. 16, pp. 508-524.

Kim, J.; Takahashi, M.; Shimizu, T.; Shirasawa, T.; Kajita, M.; Kanayama, A.; Miyamoto, Y. (2008). Effects of a Potent Antioxidant, Platinum Nanoparticle, on the Lifespan of *Caenorhabditis elegans*. *Mech Ageing Dev*, vol. 129,pp. 322-331.

Kim, W.-Y.; Kim, J.; Park, J. D.; Ryu, H. Y.; Yu, I. J. (2009). Histological Study of Gender Differences in Accumulation of Silver Nanoparticles in Kidneys of Fischer 344 Rats. *J Toxicol Env Heal A*, vol. 72, pp. 1279-1284.

Kreyling, W. G.; Semmler, M.; Erbe, F.; Mayer, P.; Takenaka, S.; Schulz, H.; Oberdörster, G.; Ziesenis, A. (2002). Translocation of Ultrafine Insoluble Iridium from Lung Epithelium to Extrapulmonary organs is Size Dependent but Very Low. *J Toxicol Environ Health*, vol. 65, pp. 1513-1530.

Krpetić, Z.; Porta, F.; Caneva, E.; Dal Santo, V.; Scarì, G. (2010). Phagocytosis of Biocompatible Gold Nanoparticles. *Langmuir*, vol. 26, pp. 14799-14805.

Könczöl, M.; Ebeling, S.; Goldenberg, E.; Treude, F.; Gminski, R.; Gieré, R.; Grobéty, B.; Rothen-Rutishauser, B.; Merfort, I.; Mersch-Sundermann, V. (2011). Cytotoxicity and Genotoxicity of Size-Fractionated Iron Oxide (Magnetite) in A549 Human Lung epithelial Cells: Role of ROS, JNK, and NF-κB. *Chem Res Toxicol*, vol. 24, pp. 1460-1475.

Larner, F.; Dogra, Y.; Dybowska, A.; Fabrega, J.; Stolpe, B.; Bridgestock, L. J.; Goodhead, R.; Weiss, D. J.; Moger, J.; Lead, J. R.; Valsami-Joner, E.; Tyler, C. R.; Galloway, T. S.; Rehkämper, M. (2012). Tracing Bioavailability of ZnO nanoparticles using Stable Isotope Labeling. *Environ Sci Technol*, vol. 46, pp. 12137-12145.

Lazaridis, M.; Dzumbova, L.; Kopanakis, I.; Ondracek, J.; Glytsos, T.; Aleksandropoulou, V.; Voulgarakis, A.; Katsivela, E.; Mihalopoulos, N.; Eleftheriadis, K. (2008). PM_{10} and $PM_{2.5}$ Levels in the Eastern Mediterranean (Akrotiri Research Station, Crete, Greece). *Water Air Soil Pollut*, vol. 189, pp. 85-101.

Lebowitz, M. D. (1996). Epidemiological Studies of the Respiratory Effects of Air Pollution. *Eur Respir J*, vol. 9, pp. 1029-1054.

Limbeck, A. ; Puls, C. ; Handler, M. (2007). Platinum and Palladium Emissions from On-Road Vehicles in the Kaisermühlen Tunnel (Vienna, Austria). *Environ Sci Technol*, vol. 41, pp. 4938-4945.

Li, H.; Jo, J. K. ; Zhang, L. D. ; Ha, C. S.; Suh, H.; Kim, I. (2010). Hyperbranched Polyglycidol Assisted Green Synthetic Protocols for the Preparation of Multifunctional Metal Nanoparticles. *Langmuir*, vol. 26, pp. 18442-18453.

Li, Y.-C. ; Yu, J. Z. ; Ho, S. S. H. ; Schauer, J. J. ; Yuan, Z. ; Lau, A. K. H.; Louie, P. K. K. (2013). Chemical Characteristics and Source Apportionment of Fine Particulate Organic Carbon in Hong kong During High Particulate Matter Episodes in Winter 2003. *Atmos Res*, vol. 120-121, pp. 88-98.

Linak, W.P. ; Yoo, J.-I. ; Wasson, S. J.; Zhu, W.; Wendt, J. O. L.; Huggins, F. E.; Chen, Y.; Shah, N.; Huffman, G. P. ; Gilmour, M. I. (2007). Ultrafine Ash Aerosols from Coal Combustion : Characterization and Health Effects. *P Combust Inst*, vol. 31, pp. 1929-1937.

Liu, Z. G.; Meng, X. K.; Guo, X. L.; Liu, X.; Liu, J. M.; Hong, J. M. (1996). The Structure of Pt-Al_2O_3 Composite Films Prepared by Pulsed Laser Deposition Technique. *Thin Solid Films*, vol. 286, pp. 49-53.

Ludwig, J.; Marufu, L. T.; Huber, B.; Andreae, M. O.; Helas, G. (2003). Domestic Combustion of Biomass Fuels in Developing Countries: A Major Source of Atmospheric Pollutants. J Atmos Chem, vol. 44, pp. 23-37.

Mahmoudi, M.; Sant, S.; Wang, B.; Laurent, S.; Sen, T. (2011). Superparamagnetic Iron Oxide Nanoparticles (SPIONs): Development, Surface Modification and Applications in Chemotherapy. *Adv Drug Deliver Rev*, vol. 63, pp. 24-46.

Mohammadnezhad, M.; Shamanian, M.; Enayati, M. H. (2012). Formation of Nanostructured NiAl Coating on Carbon Steel by Using Mechanical Alloying. *Appl Surf Sci*, vol. 263, pp. 730-736.

Monteiller, C.; Tran, L.; MacNee, W.; Faux, S. ; Jones, A. ; Miller, B. ; Donaldson, K. (2007). The Pro-Inflammatory Effects of Low-Toxicity Low-Solubility Particles, Nanoparticles and Fine Particles, on Epithelial Cells in vitro : The Role of Surface Area. *Occup Environ Med*, vol. 64, pp. 609-615.

Naqvi, S.; Samim, M.; Abdin, M. Z.; Jalees Ahmed, F.; Maitra, A. N.; Prashant, C. K.; Dinda, A. K. (2010). Concentration-Dependent Toxicity of Iron Oxide Nanoparticles Mediated by Increased Oxidative Stress. *Int J Nanomed*, vol. 5, pp. 983-989.

Nemmar, A.; Hoet, P. H. M.; Vanquickenborne, B.; Dinsdale, D.; Thomeer, M.; Hoylaerts, M. F.; Vanbilloen, H.; Mortelmans, L.; Nemery, B. (2002). Passage of Inhaled Particles Into the Blood Circulation in Humans. *Circulation*, vol. 105, pp. 411-414.

Neyshtadt, S.; Kalina, M.; Frey, G. L. (2008). Self-Organized Semiconducting Polymer-Incorporated Mesostructured Titania for Photovoltaic Applications. *Adv Mater*, vol. 20, pp. 2541-2546.

Oberdörster, G. ; Oberdörster, E.; Oberdörster, J. (2005). Nanotoxicology: An Emerging Discipline Evolving from Studies of Ultrafine Particles. *Environ Health Persp*, vol. 113, pp. 823-839.

Pabst, M. A.; Hofer, F. (1998). Deposits of Different Origin in the Lungs of the 5,300-Year-Old Tyrolean Iceman. *Am J Phys Anthropol*, vol. 107, pp. 1-12.

Pan, Y. ; Neuss, S. ; Leifert, A. ; Fischler, M. ; Wen, F. ; Simon, U.; Schmid, G.; Brandau, W.; Jahnen-Dechent, W. (2007). Size-Dependent Cytotoxicity of Gold Nanoparticles. *Small*, vol. 3, pp. 1941-1949.

Park, E.-J.; Kim, H.; Kim, Y.; Yi, J.; Choi, K.; Park, K. (2010). Inflammatory Response may be Induced by a Single intratracheal Instillation of iron nanoparticles in Mice. *Toxicology*, vol. 275, pp. 65-71.

Pazik, R.; Tekoriute, R.; Håkansson, S.; Wiglusz, R.; Strek, W.; Seisenbaeva, G. A.; Gun'ko, Y. K.; Kessler, V. G. (2009). Precursor and Solvent Effects in the Nonhydrolytic Synthesis of Complex Oxide nanoparticles for Bioimaging Applications by the Ether Elimination (Bradley) Reaction. *Chem Eur J*, vol. 15, pp. 6820-6826.

Pecora, R. (2000). Dynamic Light Scattering Measurement of Nanometer Particles in Liquids. *J Nanopart Res,* vol. 2, pp. 123-131.

Pernter, P.; Gostner, P.; Egarter Vigl, E.; Rühli, F. J. (2007). Radiologic Proof for the Iceman's Cause of Death (ca. 5'300 BP). *J Archaeol Sci*, vol. 34, pp. 1784-1786.

Perrino, C.; Canepari, S.; Cardarelli, E.; Catrambone, M.; Sargolini, T. (2008). Inorganic Constituents of urban Air Pollution in the Lazio Region (Central Italy). *Environ Monit Assess*, vol. 136, pp. 69-86.

Pillay, A. E.; Elkadi, M.; Fok, S. C.; Stephen, S.; Manuel, J.; Khan, M. Z.; Unnithan, S. (2012). A Comparison of Trace Metal Profiles of Neem Biodiesel and Commercial Biofuels using High Performance ICP-MS. *Fuel*, vol. 97, pp. 385-389.

Poland, C. A.; Duffin, R.; Kinloch, I. ; Maynard, A.; Wallace, W. A. H.; Seaton, A.; Stone, V.; Brown, S.; MacNee, W.; Donaldson, K. (2008). Carbon Nanotubes Introduced in to the Abdominal Cavity of Mice Show Asbestos-like Pathogenicity in a Pilot Study. *Nat Nanotechnol*, vol. 3, pp. 423-428.

Potgieter-Vermaak, S.; Rotondo, G.; Novakovic, V.; Rollins, S.; Van Grieken, R. (2012). Component-Specific Toxic Concerns of the Inhalable Fraction of urban Road Dust. *Environ Geochem Health*, vol. 34, pp. 689-696.

Prather, K. A.; Nordmeyer, T.; Salt, K. (1994). Real-Time Characterization of Individual Aerosol Particles using Time-of-Flight Mass Spectrometry. *Anal Chem*, vol. 66, pp. 1403-1407.

Price, O. F.; Williamson, G. J.; Henderson, S. B.; Johnston, F.; Bowman, D. M. J. S. (2012). The Relationship Between Particulate Pollution Levels in Australian Cities, Meteorology, and Landscape Fire Activity Detected from MODIS Hotspots. *PLOS One*, vol. 7, pp. 1-10.

Rauch, S.; Hemond, H. F.; Barbante, C.; Owari, M.; Morrison, G. M.; Peucker-Ehrenbrink, B.; Wass, U. (2005). Importance of Automobile Exhaust Catalyst Emissions for the Deposition of Platinum, Palladium, and Rhodium in the northern Hemisphere. *Environ Sci Technol*, vol. 39, pp. 8156-8162. *Sci Total Environ*, vol. 318, pp. 1-43.

Rauch, S.; Hemond, H. F.; Peucker-Ehrenbrink, B.; Ek, K. H.; Morrison, G. M. (2005). Platinum Group Element Concentrations and Osmium Isotopic Composition in Urban Airborne Particles from Boston, Massachusetts. *Environ Sci Technol*, vol. 39, pp. 9464-9470.

Ravindra, K.; Bencs, L.; Van Grieken, R. (2004). Platinum Group Elements in the Environment and their Health Risk. *Sci Total Environ*, vol. 318, pp. 1-43.

Riehemann, K.; Schneider, S. W.; Luger, T. A.; Godin, B.; Ferrari, M.; Fuchs, H. (2009). Nanomedicine – Challenge and Perspectives. *Angew Chem Int Ed*, vol. 48, pp. 872-897.

Shao, L.; Gao, Y.; Yan, F. (2011). Semiconductor Quantum Dots for Biomedical Applications. *Sensors*, vol. 11, pp. 11736-11751.

Silva, L. F. O.; da Boit, K. M. (2011). Nanominerals and nanoparticles in Feed Coal and Bottom Ash: Implications for Human Health Effects. *Environ Monit Assess*, vol. 174, pp. 187-197.

Singh, S. P.; Rahman, M. F.; Murty, U. S. N.; Mahboob, M.; Grover, P. (2013). Comparative Study of Genotoxicity and Tissue Distribution of Nano and Micron Sized Iron Oxide in Rats after Acute Oral Treatment. *Toxicol Appl Pharm*, vol. 266, pp. 56-66.

Song, Y.; Wang, R.; Rong, R.; Ding, J.; Liu, J.; Li, R.; Liu, Z.; Wang, X.; Zhang, J.; Fang, J. (2011). Synthesis of Well-Dispersed Aquous-Phase Magnetite Nanoparticles and Their Metabolism as an MRI Constrast Agent for the Reticuloendothelial System. *Eur J Inorg Chem*, pp. 3303-3313.

Stephen, Z. R.; Kievit, F. M.; Zhang, M. (2011). Magnetite Nanoparticles for Medical MRI Imaging. *Mater Today*, vol. 14, pp. 330-338.

Sun, J.; Simon, S. L. (2007). The Melting Behavior of Aluminum Nanoparticles. *Thermochim Acta*, vol. 463, pp. 31-40.

Sun, W.; Luna-Velasco, A.; Sierra-Alvarez, R.; Field, J. A. (2013). Assessing Protein Oxidation by Inorganic Nanoparticles with Enzyme-Linked Immunosorbent Assay (ELISA). *Biotechnol Bioeng*, vol. 110, pp. 694-701.

Syed, S.; Zubair, A.; Frieri, M. (2013). Immune Response to Nanomaterials: Implications for Medicine and Literature Review. *Curr Allergy Asthma Rep*, vol. 13, pp. 50-57.

Teja, A. S.; Koh, P.-Y. (2009). Synthesis, Properties, and Applications of Magnetic Iron Oxide Nanoparticles. *Prog Cryst Growth Ch*, vol. 55, pp. 22-45.

Totsuka, Y.; Higuchi, T.; Imai, T.; Nishikawa, A. ; Nohmi, T.; Kato, T.; Masuda, S.; Kinae, N.; Hiyoshi, K.; Ogo, S.; Kawanishi, M.; Yagi, T.; Ichinose, T.; Fukumori, N.; Watanabe, M.; Sugimura, T.; Wakabayashi, K. (2009). Genotoxicity of Nano/Microparticles in In Vitro Micronuclei, In Vivo Comet and Mutation Assay Systems. *Particle and Fibre Toxicology*, vol. 6, doi: 10.1186/1743-8977-6-23.

Tsuji, J. S.; Maynard, A. D.; Howard, P. C.; James, J. T.; Lam, C.-W.; Warheit, D. B.; Santamaria, A. B. (2006). Research Strategies for Safety Evaluation of Nanomaterials, Part IV: Risk Assessment of Nanoparticles. *Toxicol Sci*, vol. 89, pp. 42-50.

U.S. EPA (1996). Air Quality Criteria for Particulate Matter, Volume III. *United States Environmental Protection Agency, Office of Research and Development, Washington DC*, Report: EPA/600/P-95/001cF.

Venkatesh, R.; Thirumalai, K. G. Krishnan, B.; Davydov, A. V.; Merrett, J. N.; Koshka, Y. (2013). SiC Nanowire Vapor-Liquid-Solid Growth using Vapor-phase Catalyst Delivery. *J Mater Res*, vol. 28, pp. 50-56.

Wahlström, J.; Olander, L.; Olofsson, U. (2010). Size, Shape, and Elemental Composition of Airborne Wear Particles from Disc Brake Materials. *Tribol Lett*, vol. 38, pp. 15-24.

Walker Jr., B.; Mouton, C. P. (2008). Environmental Influences on Cardiovascular Health. *J Natl Med Assoc,* vol. 100, pp. 98-102.

Williams, D. B.; Carter, C. B. (2009). Transmission Electron Microscopy: A Textbook for Materials Science. *Springer Science + Business Media LLC. New York, USA*. ISBN: 978-0-387-76500-6.

Williams, D. H.; Fleming, I. (1995). Spectroscopic Methods in Organic Chemistry, 5th ed. *McGraw-Hill Publishing Company, Berkshire, U.K*. ISBN: 0-07-709147-7.

Winterstein, G.; Stahn, M.; Kühn, G. (1998). Ceramic Honeycomb Structures. *CFI Ceram Forum Int*, vol. 75, pp. 8-16.

Witasp, E.; Kupferschmidt, N.; Bengtsson, L.; Hultenby, K., Smedman, C.; Paulie, S.; Garcia-Bennett, A. E.; Fadeel, B. (2009). Efficient Internalization of mesoporous Silica Particles of Different Sizes by Primary Human Macrophages without Impairment of Macrophage Clearance of Apoptotic or Antibody-Opsonized Target Cells. *Toxicol Appl Pharm*, vol. 239, pp. 306-319.

World Health Organization (2005). WHO Air Quality Guidelines for Particulate Matter, Ozone, Nitrogen Dioxide, and Sulfur Dioxide, Global Update 2005, WHO Press, Switzerland.

Xu, W.; Ferry, M.; Cairney, J. M.; Humphreys, F. J. (2007). Three-dimensional Investigation of Particle-stimulated Nucleation in a Nickel Alloy. *Acta Mater*, vol. 55, pp. 5157-5167.

Yoshida, S.; Yasuda, M.; Miyashita, H.; Ogawa, Y.; Yoshida, T.; Matsuzaki, Y.; Tsubota, K.; Okano, H.; Shimmura, S. (2011). Generation of Stratified Squamos Epithelial Progenitor

Cells from Mouse Induced Pluripotent Stem Cells. *PLOS One*, vol. 6, doi: 10.1371/journal.pone.0028856.

Zelmanov, G.; Semiat, R. (2008). Phenol Oxidation Kinetics in Water Solution Using Iron(3)-Oxide-Based Nano-Catalysts. *Water Res*, vol. 42, pp. 3848-3856.

Zhu, M.-T.; Feng, W.-Y.; Wang, B.; Wang, T.-C.; Gu, Y.-Q.; Wang, M.; Wang, Y.; Ouyang, H.; Zhao, Y.-L.; Chai, Z.-F. (2008). Comparative Study of pulmonary Responses to Nano- and Submicron-sized Ferric Oxide in Rats. *Toxicology*, pp. 102-111.

Zou, X.; Hovmöller, S.; Oleynikov, P. (2011). Electron Crystallography: Electron Microscopy and Electron Diffraction. *Oxford University Press Inc, New York, USA*. ISBN: 978-0-19-958020-0.

Acknowledgements

I would like to give my heartfelt gratitude to my main supervisor Vadim Kessler. You are truly an inspiration when it comes to research, a great teacher and colleague. Your enthusiasm rubs off on people and this makes you a great leader. I would like to extend that gratitude to my co-supervisor Gulaim Seisenbaeva. You are a great scientist and personal inspiration, tough when needs be and kind when not required! I have learned a lot from you both and I thank you for that, *Spasiba bolshoi*.

The research in this thesis would not have been possible without the collaboration and assistance of a select few people: Johanna Lundkvist, student extraordinaire; Lena Palmberg, Bengt Fadeel, and colleagues from IMM at Karolinska Institutet for great collaborative efforts and many fruitful scientific discussions; Mats Eriksson, Julia Netrval, and Jan Magnusson of Spectral Solutions AB for generous assistance in measuring and instrument time; Karolin Guldevall from KTH for an outstanding collaboration, off the beaten path as it were, yet always enthusiastic!; Anders Gambe of Sempore AB for assistance in particle capture.

For the past 5 years I've had a great time at the department of chemistry, thanks to many great colleagues. I would especially like to mention Olesya Nikonova and Robert Pazik for good friendship and for being there when needed. Also, Anke, thank you for being a good friend. Keep it strong and keep it real, *danke schön*. As far as office buddies go, Tobias Bölscher, Felix Hentschel, Mikaela König, Sam Grice, Sarah Abtmeyer, and Samuel Paré are all deserving of a big thank you.

What would lunch-time be without bizarre discussions of disgusting topics?! Thank you lunch club: Bernt, lycka till med din kommande ledighet, glöm inte att njuta av nuet!; Lena L., tack för många trevliga diskussioner och framförallt för ditt stöd.; Shahin, du är en slitstark iransk örn, men glöm ej att

ibland ta mark.; Christina, lycka till med tant!; Johan M., du har transformerats till en stolt familjefar, lycka till med allt vad komma skall.; Eric, tack för många trevliga diskussioner och passningar på innebandyplanet. *Absit invidia*.

Jag skulle vilja tacka alla kollegor vid institutionen för kemi, ni är för många att nämna vid namn men vet vilka ni är. Särskilt tack till: Daniel, du vet mer än mig, men det vet du. Tack för att du är som du är.; David, det har varit trevligt att diskutera jobb och liv med dig.; Pierre, det har varit trevligt att ta frisk luft med dig med.; Gustav, du har utvecklats mycket sen jag lärde känna dig. Jag önskar dig lycka till med familjen.; Lars, tack för många diskussioner om allt och inget. Lycka till med nytillskottet!

Jag skulle inte ha klarat av detta arbete utan stöd från mina vänner: Emil, din lilla raggare; Niclas, så bitter! Milan, det blir slakt! Andreas, ibland får det smaka lite brunt. Tack till min närmsta familj (mor, far, Keijo och Andrew) samt mina söner Liam, Noel, Timothy och Nicholas. Tack Jessica för att du varit mitt stöd under denna resa, kunde inte ha klarat det utan dig.

Acta est fabula plaudite

2013-03-21, Uppsala